ADVANCED ENERGY MATERIALS
www.advenergymat.de

Rechargeable Battery Electrolytes Capable of Operating over Wide Temperature Windows and Delivering High Safety

*Xidong Lin, Guodong Zhou, Jiapeng Liu, Jing Yu, Mohammed B. Effat, Junxiong Wu, and Francesco Ciucci**

Li-ion batteries (LIBs) are the energy storage systems of choice for portable electronics and electric vehicles. Due to the growing deployment of energy storage solutions, LIBs are increasingly required to function safely and steadily over a broad range of operational conditions. However, the conventional electrolytes used in LIBs will malfunction when the temperatures fall below zero or elevate above 60 °C. Further, conventional electrolytes are toxic and flammable, leading to severe safety risks, especially in the case of an accident or overheating. Therefore, an ever-growing body of research has been dedicated to the development of electrolytes characterized by high ionic conductivity, excellent electrochemical stability, and operability over a wide temperature range. In this Progress Report, the optimization of liquid-based electrolytes achieved by controlling Li salts, functional additives, and solvents is discussed first. Next, gel-polymer and all-solid-state electrolytes (i.e., ceramics, polymers, and their composites) are presented. Examples of advanced batteries (Li/Na/Zn-ion batteries and Li-metal batteries) capable of working over a broad temperature window are highlighted. Morever, recent computational studies aimed at designing and understanding electrolytes are reviewed. Finally, challenges and perspectives regarding emerging electrolyte materials are proposed with the goal of triggering the further development of high-performance, safe, and wide-temperature-operating electrolytes.

1. Introduction

Energy storage technology is one of the most important pillars of low-carbon and sustainable power generation. Since Sony launched the first commercial Li-ion batteries (LIBs) in the 1990s, the technology has progressed significantly. Currently, LIBs are the most established rechargeable energy storage systems because of their high energy and power densities and low self-discharge rates.[1–3] LIBs permeate nearly every aspect of human life. They are widely used in portable electronics (e.g., smartphones, smart-watches, and laptops), transportation (e.g., electric and hybrid vehicles), and biomedical applications (e.g., cardiac pacemakers and cochlear implants). In light of these achievements, J.B. Goodenough, M.S. Whittingham, and A. Yoshino won the 2019 Nobel prize in chemistry.[4]

Despite the considerable success of conventional LIBs, their operational regime is typically around room temperature (RT). Operating at low (<0 °C) or high (>60 °C) temperatures usually deteriorate the performance and leads to safety risks.[5] We should also note that commercial LIBs are highly hazardous as they can ignite and explode in case of an accident, overheating, and overcharging, requiring more stringent safety standards, e.g., wide temperature operability and nonflammability. For example, electric vehicles require battery systems that can deliver a stable performance while maintaining a high energy density even in extreme climates, such as cold mountainous areas, where the temperatures can be as low as –40 °C, and hot deserts, where equipment exposed to sunlight can reach temperatures exceeding 70 °C.[6] Moreover, task-specific applications call for reliable energy storage solutions at extreme temperatures, including subsurface exploration (such as for mineral, oil, and gas), aerospace engineering, safety and rescue, and sterilizable medical devices.[2]

Conventional LIBs are composed of a positive electrode or cathode (e.g., $LiFePO_4$ (LFP), $LiNi_xMn_yCo_zO_2$ ($x + y + z = 1$, NMC) and $LiCoO_2$(LCO)), an electrolyte (including solvents, Li salts, and additives), a separator (typically a polyolefin membrane), and a negative electrode or anode (e.g., graphite and $Li_4Ti_5O_{12}$ (LTO)). Generally, the electrode materials are nonflammable and thermal stable (>300 °C). While the polyolefin membrane will melt/shrink over 120 °C, the commercial separators composited with ceramic nanoparticle (e.g., SiO_2 and Al_2O_3) have been developed to reduce thermal shrinkage when exposed to overheating.[7,8] Therefore, the major challenge of commercial LIBs at extreme operating temperatures comes to the electrolyte. Carbonates are commonly used as solvents for conventional LIB electrolytes. However, these compounds are

Dr. X. Lin, G. Zhou, Dr. J. Liu, J. Yu, Dr. M. B. Effat, Dr. J. Wu, Prof. F. Ciucci
Department of Mechanical and Aerospace Engineering
The Hong Kong University of Science and Technology
Hong Kong SAR, China
E-mail: francesco.ciucci@ust.hk
Prof. F. Ciucci
Department of Chemical and Biological Engineering
The Hong Kong University of Science and Technology
Hong Kong SAR, China
The ORCID identification number(s) for the author(s) of this article can be found under https://doi.org/10.1002/aenm.202001235.

DOI: 10.1002/aenm.202001235

thermally unstable, volatile, and highly flammable, critically affecting the safety of LIBs.[9] For example, at high temperature (HT), the carbonate-based electrolytes (CBEs) are chemically unstable as they react with the electrodes and PF_6^- anions disproportionately if protic impurities are present.[10–12] At low temperature (LT), the increased viscosity may reduce the ion mobility and electrode wettability, and increase the interfacial impedance, ultimately resulting in a sluggish electrochemical performance.[13,14] Further, the narrow electrochemical window of CBEs hinders their use in conjunction with high-energy-density cathode materials (e.g., NMC). Moreover, in the area of high-capacity Li-metal batteries (LMBs), conventional CBEs are unable to prevent the formation and growth of Li dendrites, a phenomenon favored by temperature.[15–17]

As LIBs with conventional CBEs may lead to device failure at extreme temperatures, alternative electrolytes have recently attracted increasing research attention. An ideal electrolyte (liquid or solid) should have specific functional properties including: i) a wide temperature tolerance; ii) nonflammability; iii) a high ionic conductivity for a wide range of temperatures; iv) a broad electrochemical window so that metal-based anodes and high-voltage cathodes can be used; v) an electrochemical and mechanical interfacial compatibility with electrodes. This review introduces such electrolytes by comprehensively examining their functional design and use in energy storage devices (**Figure 1**). First, the optimization of liquid-based electrolytes by adjusting the Li salts, additives, and solvents, is reviewed. After that, gel-polymer electrolytes (GPEs) and all-solid-state electrolytes (SSEs), e.g., ceramics, polymers, and their composites, are presented. The performance with their utilization in devices operating over a broad range of temperatures, including Li/Na/Zn-ion batteries and LMBs, are highlighted. Moreover, we review recent computational studies aimed at designing and understanding electrolytes. Finally, challenge and perspective regarding emerging electrolyte materials are proposed with the goal of triggering the further development of high-performance, safe, and wide-temperature-operating electrolytes.

Figure 1. Compositions, properties, and requirements of the electrolytes used for batteries capable of operating over wide temperature windows.

2. Liquid Electrolytes

Commercial electrolyte systems consist of a Li salt ($LiPF_6$) dissolved in a mixed solvent of carbonates, including ethylene carbonate (EC), dimethyl carbonate (DMC), diethyl carbonate (DEC), propylene carbonate (PC), and ethyl methyl carbonate (EMC).[18] The properties of common organic esters and ethers for liquid electrolytes (LEs) are summarized in **Figure 2**, where flash point (FP), boiling point (BP), and melting point (MP) are also given. These electrolytes generally are characterized by an excellent ionic conductivity (e.g., >10 mS cm^{-1}) and good wettability with the separator (i.e., polyolefin membranes) and electrodes (e.g., graphite and LFP) of the batteries.[19,20] Salts, solvents, and functional additives are the foundational components of LEs. Because they affect the performance of batteries, tuning their composition is often the first step undertaken in the electrolyte optimization process. In this section, we will review how this approach has been used to widen the temperature range.

Generally, salts/additives are used to engineer the interfaces that anode and cathode materials make with the electrolyte, which affect the operational temperature range of devices. For conventional $LiPF_6$/CBE systems, the SEI layer is composed of complex inorganic and organic mixture, including LiF, Li_2CO_3, lithium alkyl carbonates ($ROCO_2Li$) and lithium ethylene dicarbonate ($(CH_2OCO_2Li)_2$).[21–24] However, the numerous by-products and nonconductive compounds present there may lead to interfacial instability and sluggish electrochemical kinetics.[10–12] Moreover, one should note that at HT (i.e., >55 °C), parasitic reactions (e.g., $LiPF_6$ decomposition) drastically accelerate.

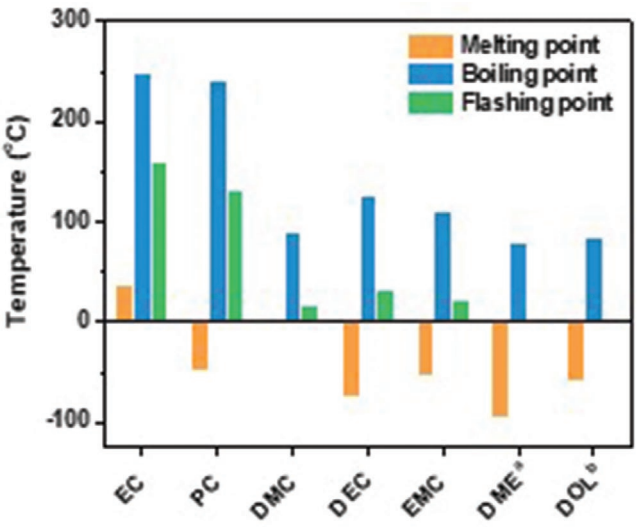

Figure 2. The melting, boiling, and flashing points of general organic esters and ethers used as LEs in batteries.[a,b] The FP of DME and DOL is 1 and 0 °C, respectively.[18]

$LiPF_6$-derived byproducts (e.g., gaseous HF and PF_5) significantly degrade the SEI, yielding CO_2, LiF, ethers, phosphates, and fluorophosphates. Meanwhile, the $LiPF_6$-derived byproducts also deteriorate the crystallinity of electrodes, and current collectors, increase the cell impedance, eventually resulting in battery failure. Several functional electrolyte components or additives, e.g., vinylene carbonate (VC),[7,25] 1,2-bis (difluoromethylsilyl) ethane (FSE),[26] and fluoroethylene carbonate (FEC)[27,28] have been used to overcome the thermal decomposition. Low concentrations of these compounds can generate protective layers over the electrode materials. For example, FEC additive results in a protective film on electrodes (e.g., LiF component on anode and polyether species on the cathode), which can effectively prevent the degradation reactions between electrolyte and electrode, and thus improve the reversibility of the battery.[29,30] Various promising Li salts, e.g., lithiumbis(oxalate)borate (LiBOB),[31,32] lithium bis(trifluoromethanesulphonyl)imide (LiTFSI),[15,16] lithium difluoro(oxalate)borate (LiDFOB)[16,33] and lithium tetrafluoro oxalate phosphate (LiTFOP),[34] have also been used to enhance the HT performance. These salts can increase the thermal decomposition temperature, optimize the SEI, and create a passivation layer that suppresses the corrosion of the current collectors.

For example, Zheng et al.[15] demonstrated that a small amount (0.05 M) of $LiPF_6$ additive in LiTFSI-LiBOB dual-salt electrolyte (EC/EMC mixed solvent) could promote the Li transfer between Li metal and electrolyte (**Figure 3**a). While the LiTFSI salt possesses high thermal stability (decomposition

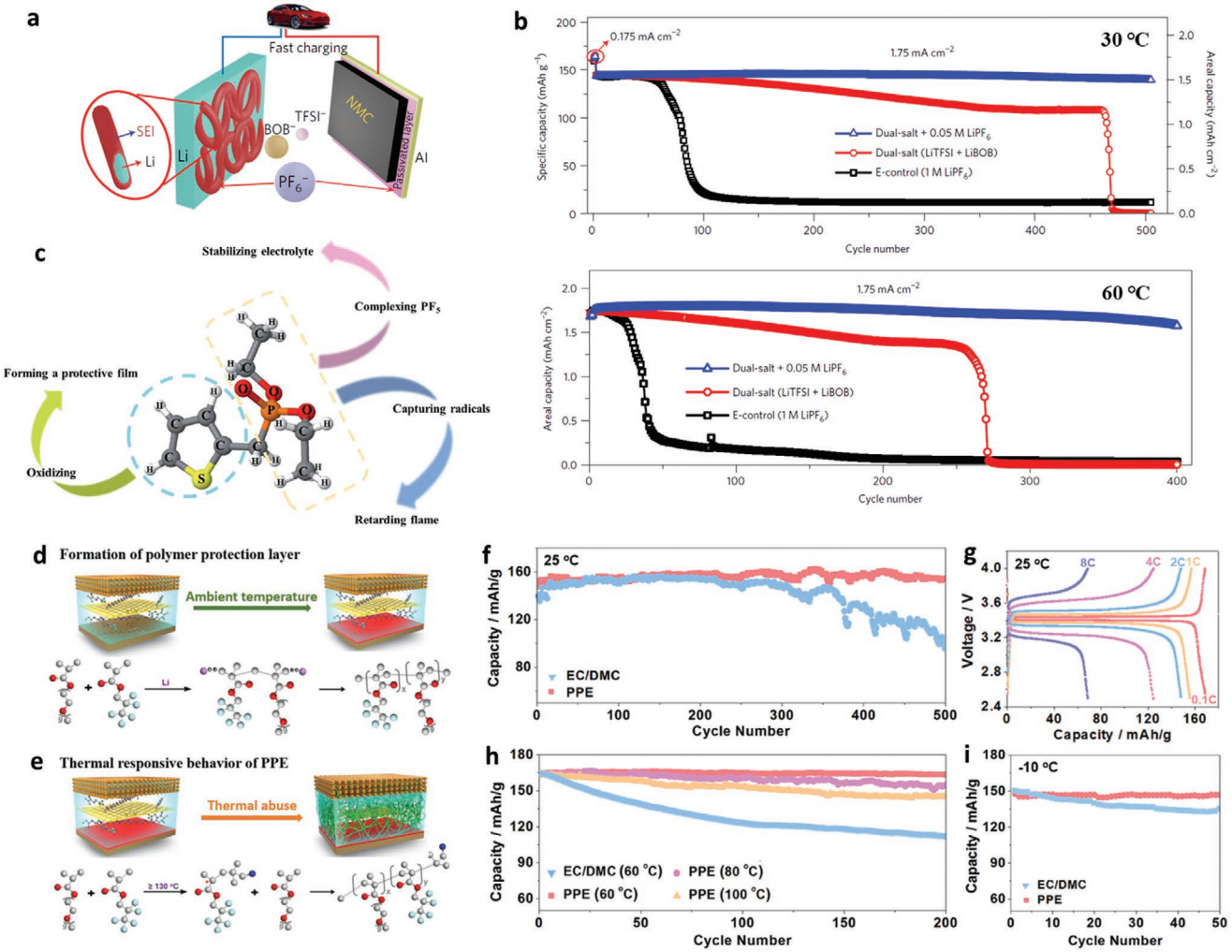

Figure 3. a) Schematic illustrating that a $LiPF_6$ additive in LiTFSI-LiBOB (dual salt) electrolyte prevents the Al corrosion and improves the stability of Li metal. b) Cycling performance of NMC/Li batteries using different electrolytes, i.e., dual-salt + 0.05 M $LiPF_6$, dual-salt, and 1 M $LiPF_6$ electrolytes, at 30 and 60 °C. Reproduced with permission.[15] Copyright 2017, Springer Nature. c) Molecular structure and functionalities of diethyl(thiophen-2-ylmethyl) phosphonate (DTYP). Reproduced with permission.[39] Copyright 2018, Royal Society of Chemistry. d) Schematic illustration of the formation of the polymeric protecting layer and the corresponding anionic polymerization mechanism on the Li electrode. e) Schematic illustration of smart PPE's thermal response behavior in the cell and the corresponding free radical polymerization mechanism under thermal abuse condition. f) Cycling performance of LFP/Li cells using PPE and $LiPF_6$-EC/DMC electrolytes for 500 cycles at 25 °C by the rate of 0.5 C. g) Typical charge/discharge curves of LFP/Li cells under the varied rate from 0.1 to 8 C. h) Cycling performance of LFP/Li cells with PPE and $LiPF_6$-EC/DMC electrolytes at elevated temperatures by 0.5 C. i) Cycling performance of LFP/Li cells using PPE and $LiPF_6$-EC/DMC electrolytes at –10 °C by the rate of 0.1 C. Reproduced with permission.[44] Copyright 2020, John Wiley and Sons.

temperature as high as 343 °C) and can tolerate some water contamination, it corrodes Al foil.[32] Not only that, the corrosion by-product $Al(TFSI)_3$ could deposit on the electrodes and affect the device performance. The introduction of LiBOB enabled the formation of a borate-containing passivation film that prevented such corrosion from taking place. The $LiPF_6$ additive of LiTFSI-LiBOB dual-salt electrolytes also helped form a Li-conductive polycarbonate-rich SEI, which protected Li metal against the electrolyte. As a result, at a high current density of 1.75 mA cm^{-2} (30 °C), the NMC/Li batteries with $LiPF_6$-added LiTFSI-LiBOB dual-salt electrolyte delivered impressive capacity retention (>97%) after 500 cycles. In comparison, the conventional $LiPF_6$ electrolyte and LiTFSI-LiBOB dual-salt electrolyte exhibited sharp capacity drop after 60 and 450 cycles, respectively. The capacity degradation has been attributed to the formation of an unstable SEI, which is not only fragile and resistive but also results in a continuous reaction between Li and electrolyte. At 60 °C, Li/NMC batteries with $LiPF_6$-added dual-salt electrolyte could sustain over 400 cycles at 1.75 mA cm^{-2} while delivering 147 mAh g^{-1}. Instead, the batteries using the other two electrolytes presented a fast capacity loss due to the degradation of the Li metal surface (Figure 3b).

Recently, significant research effort has been dedicated to making CBEs less flammable by using flame-retarding additives, e.g., phosphorus-based flame retardant trimethyl phosphate (TMP),[35] triphenyl phosphate (TPP),[36] and triethyl phosphate (TEP).[37,38] For example, TPP can produce phosphorus-containing free radicals, such as $PO^{\bullet}$ and $PO_2^{\bullet}$, which can capture the $H^{\bullet}$ and $HO^{\bullet}$ radicals released from the burning composition. Therefore, the combustion chain branching reactions can be weakened or terminated. Li and co-workers[39] used diethyl(thiophen-2-ylmethyl)phosphonate (DTYP) as a multifunctional additive for high-voltage LIBs (Figure 3c). DTYP was composed of thiophene and phosphate. The thiophene could form ionically conductive cathode interphases via the polymerization of the thiophene radical due to its preferential oxidation. The oxygen in the phosphate group could neutralize PF_5 derived from $LiPF_6$ via acid-base coordination. Further, the DTYP could effectively act as a flame-retarding agent. The transition metal dissolution and deposition onto the anode, which deteriorates the battery performance, could be prevented by the presence of DTYP. Remarkably, with only 5% of DTYP in EC/EMC, the thermal stability and the interfacial stability between $LiNi_{0.5}Mn_{1.5}O_4$ and electrolyte improved. The DTYP-containing $LiNi_{0.5}Mn_{1.5}O_4$/Li cells demonstrated a superior rate capability compared to analogous batteries with CBEs by delivering a capacity of 93 mAh g^{-1} at RT and 15 C (vs 57 mAh g^{-1}) and an 85% capacity retention at 60 °C and 1 C over 280 cycles (vs 18%).

The electrolyte solvent plays a crucial role in regulating the solvation sheath of Li-ions, the construction of cathode/anode-electrolyte interphases, and the insertion of Li-ions inactive materials.[18] An ideal electrolyte should be considered by i) good solvation to dissolve Li salt; ii) chemical inertness toward battery materials; iii) a low viscosity (<1 mPa s at RT) to favor ion mobility; iv) a wide electrochemical window (>4.5 V vs Li^+/Li); v) a low MP (<0 °C) and a high BP and FP (>100 °C) to enhance safety and extend the operating temperature window.[40] Carboxylate esters, such as ethyl propionate, ethyl acetate, methyl butyrate, and methyl acetate, have been used as cosolvents to extend the operating temperature.[41,42] Also, fluorinated solvents, such as FEC, favor the formation of thermally stable SEI layers, significantly expanding the cyclic stability at HT operation.[28,43]

EC/PC mixtures have been used as solvents due to their high boiling point (>200 °C) and excellent flame resistance. Kohlmeyer et al.[7] developed a unique nanocomposite membrane with an HT electrolyte (Pyrolux/HT) capable of operating over a wide temperature window (20–120 °C). The membrane was based on a printable and flexible Al_2O_3-poly(vinylidene fluoride) separator infiltrated by an EC/PC mixture solvent. At 20 °C, both Pyrolux/HT and a conventional system (Celgard/$LiPF_6$) exhibited comparable performance at 0.33 C (≈130 mAh g^{-1}) and Coulombic efficiency (CE) ≥99.5%. At 120 °C, the Celgard/$LiPF_6$-based battery failed during the first cycle. However, LFP/Li and Li/graphite half-cells with the Pyrolux/HT system achieved reversible capacities of 155 and 340 mAh g^{-1}, respectively, with CE > 99.4%. In a recent article, the Li group[16] reported an HT electrolyte combining a LiTFSI-LiDFOB dual salt and a mixture of EC/PC solvents. 0.01 M of $LiPF_6$ was also employed to mitigate the corrosion of the Al current collector from the LiTFSI salt. The resulting LCO/Li cells delivered effectively enhanced cyclic stability with a capacity of 2.4 mAh cm^{-2}, even at 80 °C. The improved electrochemical performance at elevated temperature was attributed to the excellent thermal stability of electrolyte, and the high quality of the SEI film, which, among other beneficial effects, inhibits the growth of Li dendrites during cycling.

Recently, the Cui group[44] developed a temperature-responsive electrolyte (denoted as PPE) that included liquid polymer monomers, i.e., poly(ethylene glycol) methyl ether methacrylate (PEGA) and 2,2,3,3,3-pentafluoropropyl acrylate. Such a composition triggered two kinds of polymerization reactions that could, in turn, improve the safety of LMBs (Figure 3d-i). First, a polymer protection layer on Li metal was formed by anionic polymerization, significantly inhibiting the growth of Li dendrites and contributing to the long-term Li plating/stripping cyclability (up to 2000 h). At 130 °C, the electrolyte rapidly transformed from a liquid into a solid via a thermal-free radical polymerization. The remarkable feature was that the thermal decomposition temperature increased to 350 °C. The PPE had an ionic conductivity of 2.28 mS cm^{-1} at RT. LMBs employing this electrolyte could cycle effectively over a wide temperature range from –10 to 100 °C. For example, the LFP/Li cell delivered a discharge capacity of 151 mAh g^{-1} (0.1 C) and a high CE of 99.6% after 500 cycles at 25 °C. Meanwhile, the LFP/Li cells exhibited capacities of 148 and 145 mAh g^{-1} at –10 and 100 °C, respectively.

Ionic liquids (ILs) are a very interesting class of RT molten salts.[45] ILs consist of large and asymmetrical organic cations (e.g., imidazolium, pyridinium, and piperidinium) and anions (e.g., BF_4^-, PF_6^-, and $TFSI^-$). ILs are promising electrolyte candidates for highly safe devices, because of their nonflammability, chemically, and electrochemically stability (up to 5 V vs Li^+/Li), nonvolatility, and remarkable thermal stability (300–400 °C).[40,46–52] For example, Elia et al.[53] reported an IL-based electrolyte composed of *N*-butyl-*N*-methylpyrrolidinium bis(fluoro-sulfonyl)imide [Pyr14][FSI]. Such IL-based electrolytes introduced robust SEI, and thus contributed to the exceptionally

long lifespan for LFP/Sn-C cell (2000 cycles, 40 °C). Recently, the Ajayan group[54] leveraged these properties to formulate a piperidinium-based IL electrolyte capable of reaching an ionic conductivity of 3 mS cm^{-1} at RT. The as-designed ionic-liquid-based electrolyte allowed the stable operation of LTO/Li cell from 24 to 150 °C, e.g., ≈90 mAh g^{-1} over 40 cycles at 24 °C (C/8) and ≈140 mAh g^{-1} over 600 times at 120 °C (3 C). While ILs have outstanding thermal stability and safety, their high cost, low ionic conductivity (typically < 0.1 mS cm^{-1} at RT), and high viscosity remain a barrier for the practical applications.

Commercially available LIB cathode materials, such as LFP, LCO, and $LiMn_2O_4$ (LMO), typically deliver specific capacities lower than 170 mAh g^{-1}. NMC cathodes, depending on the composition, possess high theoretical specific capacities in the 274–285 mAh g^{-1} range. However, due to the limited structural stability and lattice oxygen oxidation, they practically deliver less than 200 mAh g^{-1}. Therefore, the cathode material is one of the biggest bottlenecks of high-energy-density LIBs. Li-S batteries (LSBs) have been extensively investigated due to their high theoretical energy density (2600 Wh kg^{-1}) and potentially low cost due to the abundance of sulfur.[55–59] Nonetheless, the safety of LSB technology remains a challenge, especially because of the presence of flammable organic solvents, polysulfide shuttle, and the uncontrollable growth of Li dendrites.[16,18,60] To realize high performance and safe LSBs, the Wang group[38] developed a nonflammable electrolyte consisting of lithium bis(fluorosulfonyl)imide (LiFSI) and a flame-retarding co-solvent composed of 1,1,2,2-tetrafluoroethyl-2,2,3,3-tetrafluoropropyl ether (TTE) and TEP. TTE lowered the viscosity of the electrolyte, thereby increasing its effective ionic conductivity. Meanwhile, TEP was highly coordinated with LiFSI, and lithium polysulfides could bind to fewer free solvent molecules. In addition, the presence of TEP induced a Li_3PO_4-based and LiF-rich layer on both anode and cathode. Such a protective layer could effectively regulate the dendrite-free deposition of Li and suppress side reactions between the electrolyte and sulfur, thereby guaranteeing long-term cyclic stability. At a current density of 0.5 C, the LSBs with this electrolyte were able to achieve 418.1 mAh g^{-1} (1000 cycles) and 751.8 mAh g^{-1} (100 cycles) at RT and 60 °C, respectively. In contrast, the capacity of LSBs with a conventional electrolyte decayed quickly.

LIBs suffer severe power loss if the temperatures fall below 0 °C due to the decreasing ionic conductivity, increasing viscosity, and freezing of the electrolyte.[13,61] Low-melting-point and low-viscosity solvents, e.g., ethyl acetate (EA) with −84 $°C_{MP}$ and dichloromethane (DCM) with −95 $°C_{MP}$, are generally used to guarantee the workability of the cell. For example, Dong et al.[62] reported an EA/DCM cosolvent electrolyte for LMBs, which possessed a high ionic conductivity (0.6 mS cm^{-1}), low viscosity (0.35 Pa s), and wide range of potential window (0–4.85 V) even at −70 °C. Also, interface film-forming additives (e.g., FEC,[63] butyl sultone,[64] and $LiBF_4$[65]) are employed to stabilize the electrode/electrolyte interfaces by constructing high-density and Li-conducting passivation films that improve Li transfer.[31,66] For example, Smart et al.[41] reported that the addition of 20 vol% methyl propionate or ethyl propionate to EC/DMC mixtures enabled a 70% capacity retention when the cell was operated at −60 °C.

The Zhang group[27] introduced $LiNO_3$ and FEC concurrently into an electrolyte to regulate the solvation sheath of Li ions and generate a homogeneous SEI with abundant LiF and LiN_xO_y for the dendrite-free deposition of Li (**Figure 4**a–c). Consequently, when operating at RT, the LFP/Li battery with the FEC/$LiNO_3$ electrolyte had a high CE of 99.96% and could be cycled 1000 times. Moreover, at −10 °C the batteries with the FEC/$LiNO_3$ electrolyte exhibited better rate performance than those with the EC/DEC electrolyte (80 vs 50 mAh g^{-1} at 0.5 C). When the working temperature increased to 60 °C, the cells with the EC/DEC electrolyte quickly decayed after 25 cycles at 1 C. In contrast, the FEC/$LiNO_3$ electrolyte allowed for a stable battery operation over 180 cycles.

Li and co-workers[67] reported that the cyclic stability of high-energy batteries at LT could be enhanced by adding lithium difluorobis(oxalato) phosphate (LiDFBOP). Protective interfacial films generated simultaneously on both electrodes by the reduction and oxidation of LiDFBOP. Such protection prevented the electrolyte decomposition and allowed the formation of a low-impedance SEI. Therefore, NMC/graphite batteries displayed a superior cyclic ability at both RT and LT. Even below −30 °C, the cells containing LiDFBOP retained a much higher portion of their RT capacity (49%) compared to those with a conventional electrolyte (14%).

The Wang group[68] developed a class of electrolytes by dissolving fluorinated electrolytes, including FEC and methyl (2,2,2-trifluoroethyl) carbonate (FEMC), into highly fluorinated nonpolar solvents, such as methoxyperfluorobutane and tetrafluoro-1-(2,2,2-trifluoroethoxy)ethane as shown in Figure 4d–j. Such electrolytes maintained the superior properties of the fluorinated component, including the generation of LiF-rich SEI on the Li surface, nonflammability, and the widening of the electrochemical potential window. Further, the fluorinated polar carbonate solvents in the super-electrolyte provided a high conductivity (>1 mS cm^{-1}). These highly fluorinated and nonpolar solvents had a much lower molecular interaction, breaking the affinities between the solvents and ions, and ensuring a wide liquid-phase temperature range, low viscosity, and low Li^+ desolvation energy. Consequently, the resulting electrolytes had a high ionic conductivity in a wide temperature range from −125 to +70 °C (e.g., 0.011 mS cm^{-1} at −80 °C, 2.3 mS cm^{-1} at 25 °C, and 3.5 mS cm^{-1} at 60 °C) and high electrochemical stability in a wide potential window from 0.0 to 5.6 V. The $LiNi_{0.8}Co_{0.15}Al_{0.05}O_2$/Li cells with this super-electrolyte had similar capacities of 172 mAh g^{-1} at RT regardless of the electrolyte composition among those investigated. When the temperature was reduced to −42 °C, the conventional carbonate electrolyte completely solidified. The cell using this carbonate electrolyte delivered a low capacity of 13.3 mAh g^{-1}. Instead, the super electrolyte-based cell still had a high capacity of 160 mAh g^{-1}.

Liquefied gas is a special solvent. Generally, liquefied gas remains a gaseous state at RT, but it can liquefy under cooling or pressure. Hydrofluorocarbon liquefied gas, e.g., fluoromethane (FM) and difluoromethane (DFM), is proposed as a solvent for LIBs since its high electrochemical stability and exceptional low viscosities over a wide range of temperatures (e.g., $\eta_{DFM,\ -60\ °C}$ = 0.31 mPa s and $\eta_{DFM,\ 20\ °C}$ = 0.12 mPa s). Therefore, the liquefied gas is expected to employ at ultra LT where CBEs may freeze. Recently, the

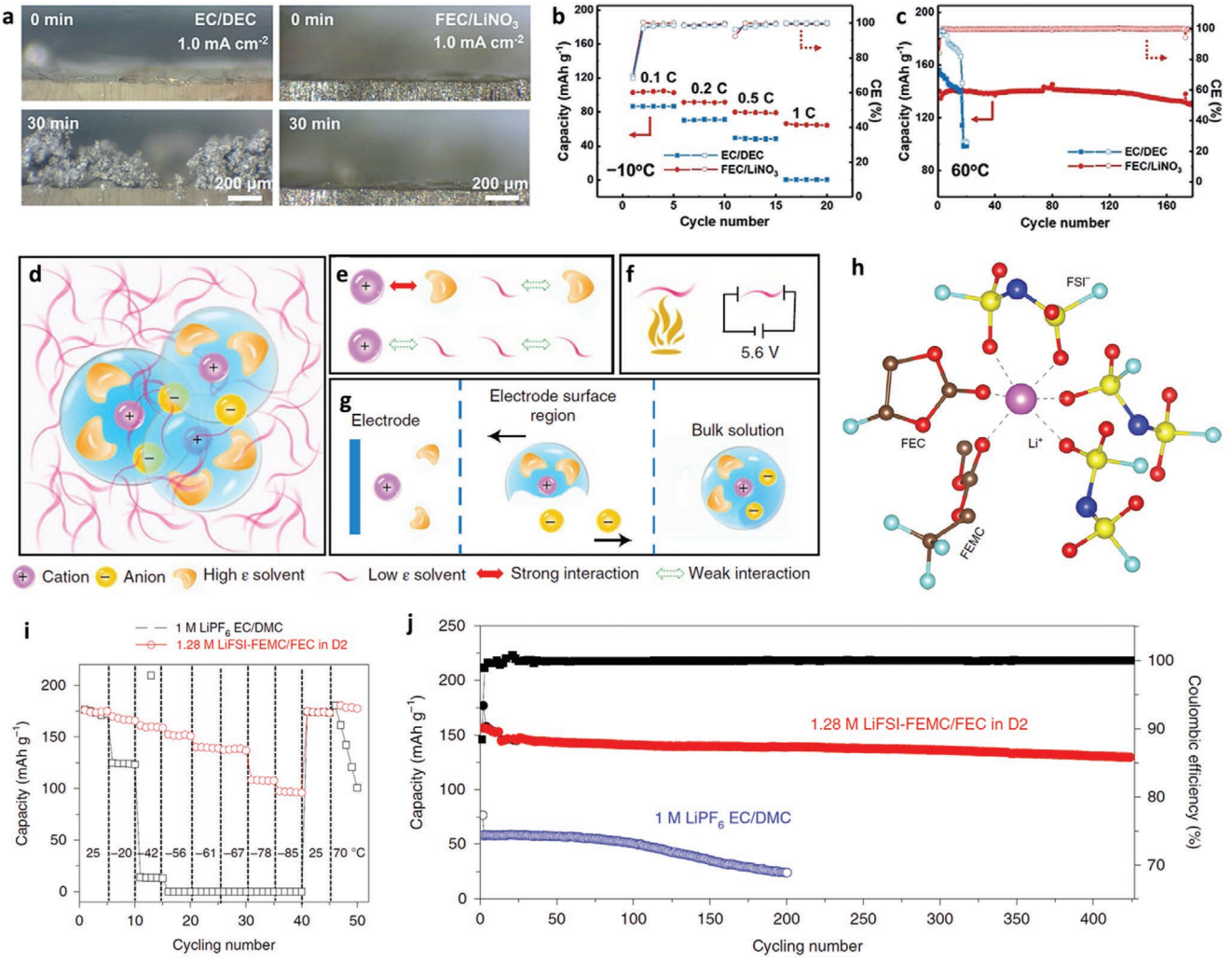

Figure 4. a) In situ optical microscopy observations of Li deposition process in EC/DEC and FEC/$LiNO_3$ electrolytes at 1.0 mA cm^{-2}. b) Rate capability and CE of LFP/Li coin cells at −10 °C at 1.0 C, and c) HT performance of LFP/Li coin cells at 60 °C and corresponding CE at 1.0 C. Reproduced with permission.[27] Copyright 2018, John Wiley and Sons. d) The electrolyte uses a nonpolar solvent to tame the fluorinated carbonate electrolytes. e) The affinities between the solvents and ions. The Li-ions and fluorinated carbonate solvents have a strong interaction, while the other three species have weak interactions between each other. f) The nonflammable and high electrochemical stability requirements for the nonpolar solvent in the super electrolyte. The nonpolar solvents are nonflammable and can withstand an extremely high voltage of 5.6 V. g) The expected electrochemical process at the electrode and electrolyte interface of the tamed electrolyte. In the bulk electrolyte, the Li ions will be solvated by fluorinated carbonate molecules and anions. At the surface region, the solvated Li ions will separate from the anions using the electric field. As the Li-ions arrive at the surface of the electrode, the fluorinated carbonate molecules will finally be desolvated. h) The representative Li^+ solvation structure extracted from the cMD simulations. i) Discharge capacities of $LiNi_{0.8}Co_{0.15}Al_{0.05}O_2$/Li cells using 1.28 M LiFSI-FEC/FEMC-D2 and 1.0 M $LiPF_6$-EC/DMC electrolytes at different temperatures. j) Cycling performance of $LiNi_{0.8}Co_{0.15}Al_{0.05}O_2$/Li using 1 M $LiPF_6$-EC/DMC and 1.28 M LiFSI-FEC/FEMC-D2 electrolytes at −20 °C with a charge/discharge current density of 1/3 C. Reproduced with permission.[68] Copyright 2019, Springer Nature.

Meng group developed a variety of unique liquefied gas electrolyte based on hydrofluorocarbons.[69–71] Typically, the gaseous hydrofluorocarbons were first liquefied under pressure and subsequently dissolved Li salts to procedure liquid-state electrolytes in high pressure stainless steel cells. These novel electrolytes demonstrated good Li-metal compatibility and impressive operation window (e.g., −60 to +55 °C). For example, they recently designed an FM-based electrolyte for high-voltage LMBs utilizing acetonitrile (AN) as cosolvent.[71] The introduction of AN significantly improved the dissolubility of LiTFSI, and therefore increase more coordination of FM-Li^+. When salt concentrations increased above 1 M, AN was fully solvated with Li cations with barely free molecules, which could improve the electrochemical stability of electrolyte. Meanwhile, the FM-Li^+ coordination provided much shorter residence time (32 ps, 0 °C) for than Li-AN (7407 ps) and Li-N(TFSI) (6926 ps), indicating the rapid ion transport and desolvation even at LT. Due to the excellent conductivity (>4 mS cm^{-1}) from −78 to +75 °C and high transference number (0.72 at RT), the liquefied gas electrolyte delivered outstanding Li-metal stability with a high average CE (99.4%) at 3 mA cm^{-2} (3 mAh cm^{-2}, 200 cycles) and impressive performance of 4.5 V NMC/Li batteries between −60 to +55 °C, e.g., ≈120 mAh g^{-1} (C/15) at −40 °C.

The limited lithium resources and high cost of lithium ore remain limiting factors, especially for electric vehicles and grid-scale energy storage systems. Therefore, it is essential and urgent to develop rechargeable batteries based on earth-abundant elements. Among them, sodium is a promising candidate.[72,73] Due to the size and mass of the Na^+ cation, the energy and power densities of sodium-ion batteries (SIBs) are significantly reduced when the temperature falls below 0 °C. Several studies have addressed this issue by making high-performance SIBs capable of operating at sub-zero temperatures. You et al.[74] and Guo et al.[75] developed cathodes for SIBs that can work at temperatures as low as –25 °C. Wang et al.[76] and Hou et al.[77] made anodes based on carbon nanomaterials and analyzed their electrochemical performance in the temperature range from –25 to 25 °C. In the above articles, the electrolyte consisted of $NaClO_4$ or $NaPF_6$ dissolved in carbonates (EC, PC, and FEC). Due to the freezing point of the solvent (35–38 °C for EC, –48 °C for PC, and 18 °C for FEC) and the increased viscosity at decreasing temperature, the performance at temperatures below –25 °C was limited.

So far, we have discussed electrolytes based on organic solvents. However, most organic solvents are intrinsically flammable, which poses safety concerns, especially for HT applications. Because of the high ionic conductivity (1–10 S cm^{-1} at RT),[78] intrinsic nonflammability, environmental friendliness, and low cost of water-based electrolytes, aqueous batteries have been studied extensively. As is well known, the freezing point of water is 0 °C at atmospheric pressure. Under these conditions, H_2O molecules crystallize due to the hydrogen bonds. Incorporating dimethylsulfoxide (DMSO), a sulfur-containing molecule, into H_2O can disrupt the hydrogen bond network, thereby lowering the freezing point. Nian et al.[79] prepared an electrolyte with a freezing point lower than –130 °C by adding DMSO in a molar fraction of 0.3. Using $NaTi_2(PO_4)_3$@C (NTP) as an anode and activated carbon as a cathode, the same group made a full battery that delivered 68 mAh g^{-1} at –50 °C at a rate of 0.5 C (1 C = 133 mA g^{-1}). Fourier transform infrared (FTIR) and Raman spectral characterization, as well as molecular dynamics (MD) simulations, suggested that the hydrogen bond network was formed between the oxygen atom in the S=O bond and the hydrogen atom in the O—H bond, preventing the formation of the ice crystals.

Among them, zinc is another attractive candidate due to its low cost and high specific capacities (about 820 mAh g^{-1}). Zinc ion batteries (ZIBs) suffer from limited cycling stability because of the cathode structure collapse, anode dendrite formation, and hydrogen evolution. To solve these problems, Wang et al.[80] prepared a zinc-organic battery with a phenanthrenequinone macrocyclic trimer (PQ-MCT) cathode, a zinc-foil anode, and a nonaqueous electrolyte with *N*,*N*-dimethylformamide (DMF). The organic cathode could store Zn^{2+} ions through a reversible coordination reaction with fast kinetics, while the nonaqueous nature of the system and the formation of a Zn^{2+}-DMF complex was able to efficiently eliminate undesired hydrogen evolution and dendrite growth on the Zn anode. Therefore, this battery could cycle 20 000 times with negligible capacity decay. Furthermore, due to the low MP and high BP of DMF, it could be operated in the temperature range from –70 to 150 °C, achieving 31.3 and 196 mAh g^{-1} at –70 and 150 °C, respectively.

While the emerging LEs enhance the safety of rechargeable batteries and deliver wide temperature operation, they have issues that need resolving. First, fluorine-containing solvents and ILs can be utilized to design safer batteries, but costs can be high. Low-cost alternatives should be further developed. Second, the additives are not only adopted to facilitate stable SEI but also expected to possess additional functionalities, such as capabilities to extinguish fires. Aqueous electrolytes that are intrinsically environmentally friendly, inexpensive, and safe are promising alternatives to the toxic and flammable CBEs. Expanding the effective electrochemical and temperature windows of aqueous electrolytes is one exciting research direction.

3. Gel Polymer Electrolytes

Conventional LEs have been widely used due to their high ionic conductivities, but their leakage leads to severe safety concerns. GPEs, which are a mixture of polymers, solvents, salts, and other constituents, can overcome the challenges inherent to LEs. In particular, GPEs combine the advantages of LEs and polymer, including good contact with electrodes, relatively high ionic conductivities, and flexibility.[81,82] The polymer framework in GPEs serves as a host material and provides the mechanical strength, while the salt is the source of charge carriers. The solvent, which is added to dissolve polymers and salts, enables the segmental motion and promotes the dissociation of the salt. Also, the polymer chains immobilize the solvent.[81] GPEs not only prevent the leakage of the LE but also possess a higher ionic conductivity than SPEs. As the properties of GPEs are determined by the composition and the preparation method,[83–86] efforts have been made to improve the performance of GPEs by fine-tuning the formulation and synthesis. Several strategies have been proposed to enhance the thermal stability and safety of GPEs. These include grafting thermally stable molecular chains,[87] adding thermally stable plasticizers,[88] introducing inorganic particles,[89–94] and using ionic liquid or poly(ionic liquid)s (PILs).[95–101] There are two commonly used methods to fabricate GPEs. The first one is called solution casting, which involves the dissolution of polymer and the subsequent casting and solvent evaporation. While this method has been widely adopted, the consumption of large amounts of solvents raises cost and pollution issues. Besides, it is difficult to precisely control the film-formation process, which makes it hard to produce GPEs reliably. Another intensively investigated method is the in situ formation of GPEs. Polymer precursors, including the monomer/oligomer/linear polymer, cross-linker, and initiator are mixed along with solvents into a homogeneous solution and form a GPE subjected to heat[102–104] or UV treatment.[105–110] The polymerization process could also be carried inside the battery in the case of thermally induced curing. UV-curing is a facile method to prepare GPEs under RT efficiently. For example, Porcarelli et al.[111] architecture a super soft polymer electrolyte network directly on TiO_2 and LFP electrode by in situ UV treatment of linear poly(ethylene oxide) (PEO) with different molecular weights (**Figure 5**a). An optimized cathode/electrolyte interface was achieved by in situ polymerization, which reduced the interfacial resistance. The resilient GPE with

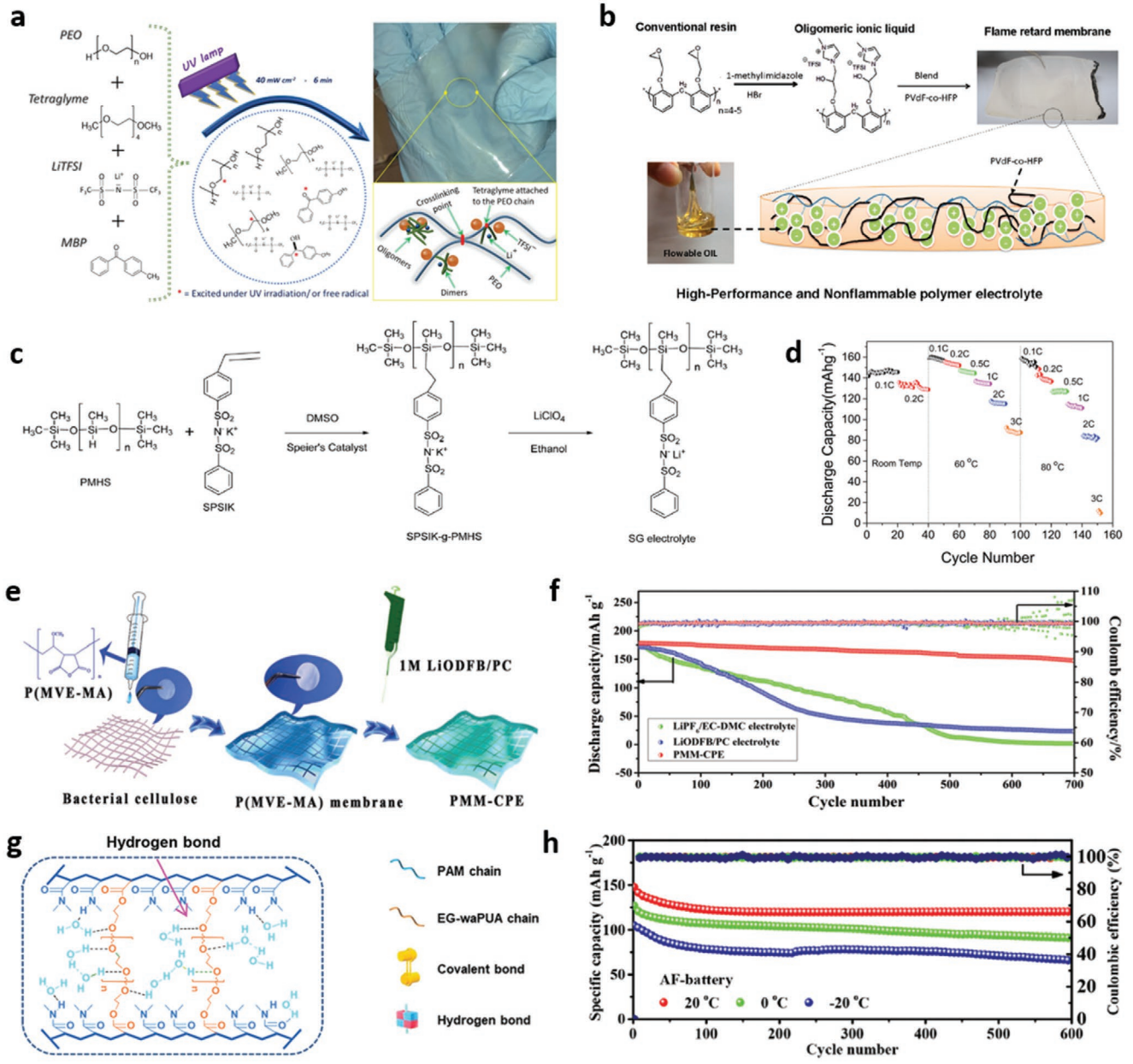

Figure 5. a) Sketched representation of soft polymer electrolyte network prepared by UV-curing. Reproduced with permission.[111] Copyright 2016, Springer Nature. b) Preparation and schematic of the GPE based on oligomeric IL. Reproduced with permission.[97] Copyright 2016, Elsevier. c) Polysiloxane-based SIPE and d) its electrochemical performances at RT and HT. Reproduced with permission.[121] Copyright 2015, Royal Society of Chemistry. e) Schematic representation of the PMM-CPE fabrication process and f) it's cycling performance of the 4.45 V-class $LiCoO_2$/Li cell at 1 C and 60 °C. Reproduced with permission.[122] Copyright 2018, Royal Society of Chemistry. g) Schematic illustration of the strong hydrogen bonds between EG-waPUA, water and PAM in the anti-freezing hydrogel and h) the cycling performance of the anti-freezing battery at 2.4 A g^{-1} at different temperatures. Reproduced with permission.[124] Copyright 2019, Royal Society of Chemistry.

tetraglyme plasticizer eliminated dendrite-induced short circuit and enabled stable cycling of the symmetric cell for more than 500 h at 0.2 mA cm^{-2}.

As already outlined in the section above, ionic liquids are potential candidates for high-performance electrolytes due to their high ionic conductivity (10^{-4}–10^{-2} S cm^{-1}),[112] electrochemical stability, nonflammability, and nonvolatility.[113–118] Therefore, they have been intensively investigated in the application of GPEs both experimentally[95–101] and theoretically.[119,120] Kuo et al.[97] synthesized oligomeric IL from conventional phenolic epoxy resin (Figure 5b). By blending the oligomeric ionic liquid with poly(vinylidene fluoride-*co*-hexafluoropropylene) (PVDF-HFP), they made high performance and nonflammable GPE. The GPE possessed high ionic conductivities of 2.0×10^{-3} and 6.6×10^{-3} S cm^{-1} at 30 and 80 °C, respectively. A battery made of the GPE, Li metal, and LFP delivered rate capabilities of 152 mAh g^{-1} at 0.1 C and 141 mAh g^{-1} at 1 C. Due to the presence of the oligomeric ionic liquid, the novel GPE displayed

superior dimensional stability at 150 °C and a limiting oxygen index (the minimum oxygen volumetric content needed to sustain burning) as high as 29. Both properties lead to a safer gel.

Rohan et al.[121] designed, based on polysiloxane, a single ion conducting polymeric electrolyte (SIPE) that was thermally stable up to 410 °C (Figure 5c). Styrenesulfonyl(phenylsulfonyl)imide groups were grafted on the backbone of the polysiloxane. The SIPE was then mixed with PVDF-HFP and soaked in EC/PC to make a GPE. Because of the highly delocalized anionic charges on the side groups, the Li-ions readily dissociated. The ionic conductivity of the GPE reached 7.2×10^{-4} S cm^{-1} at RT and the t_{Li+} was close to 0.89. The LFP/GPE/Li cell displayed a 0.1 C capacity of 141, 159, and 154 mAh g^{-1} at RT, 60 and 80 °C, respectively (Figure 5d).

Dong et al.[122] designed a multifunctional polymer electrolyte (Figure 5e), named PMM-CPE for a high-voltage LCO/PMM-CPE/Li cell (up to 4.45 V). PMM-CPE included a bacterial cellulose substrate, poly(methyl vinyl ether-*alt*-maleic anhydride), and PC/lithium difluoro(oxalato) borate (LiODFB). PMM-CPE served as an effective protection layer on LCO and a robust SEI film on the Li anode. Further, PMM-CPE had a high ionic conductivity (>10^{-3} S cm^{-1} at 30 °C) and a wide electrochemical window (up to 5.2 V vs Li^+/Li). The resulting LCO/PMM-CPE/Li cell exhibited outstanding cyclic stability at 25 °C (73% after 650 cycles) and 60 °C (85% after 700 cycles), see Figure 5f. Both values are significantly better than those with conventional electrolytes. As discussed in Section 2, aqueous batteries are fascinating due to the low cost and high safety. However, Li, Na, or K metal anode could not be directly used because of the high reactivity of aqueous electrolyte. Therefore, the lack of high capacity anode is a major obstacle to the improvement of the energy density of aqueous batteries. ZIBs have drawn considerable research interest due to their high specific capacities (about 820 mAh g^{-1}), low cost of Zn compared with Li, and stability in water. However, using GPEs below 0 °C remains a significant challenge. Zhu et al.[123] prepared an anti-freezing hydrogel by dissolving $ZnSO_4$ and LiCl in the acrylamide aqueous solution. The hydration of Zn^{2+}, SO_4^{2-}, and Li^+ eliminated the intermolecular hydrogen bonds, suppressing the freezing of water at temperatures as low as −20 °C. The battery based on the anti-freezing hydrogel electrolyte, LFP and Zn displayed highly stable cycling performance at −20 °C. Mo et al.[124] prepared an anti-freezing hydrogel electrolyte by incorporating ethylene glycol, a well-known anti-freezing agent, into the polymer network (Figure 5g). Ethylene glycol disrupted the hydrogen bond network among H_2O molecules, inhibiting the formation of ice crystals and decreasing the vapor pressure. Therefore, flexible ZIBs could work at −20 °C for 500 cycles at 0.5 A g^{-1} while preserving 82.18% of their initial capacity (Figure 5h).

Despite the great progress achieved by GPEs, several issues still need to be addressed. First, while the leakage problem is inhibited, the GPEs still confine high-content flammable liquid, which is unsafe for HT operation. One effective solution is to embed thermally stable and flame-retarding additives, solvents, and polymers into the GPEs. Secondly, the liquid content leads to the tradeoff between safety and electrochemical performance. It is important to design the whole GPEs system with the guidance of scientific insight, such as free volume, solubility parameter, and polymer crystallinity theories, while the solvation of charge carriers, polymer-cation interaction, and polymer-anion interaction also need to be taken into account when choosing the GPE components at the same time. Moreover, the fabrication of thin free-standing GPE is challenging. The in situ formation of GPEs often involves thermal treatment lasting several hours. Such a treatment might lead to side reactions or dissolution of electrode materials in liquid precursors. The in situ UV-curing is a promising method because it is carried out at RT over a short time (from a few seconds to a few minutes) without significant temperature increase. Furthermore, within this method, the thickness can be adjusted by the incorporation of the porous support. However, one needs to carefully choose the GPE monomers and cross-linkers in order to achieve ease of UV-curing, stability toward anode and cathode, HT stability/LT ionic conductivity, and high electrochemical performance.

4. Solid-State Electrolytes

LEs and GPEs contain liquids, which still has a risk of leakage, corrosion, ignition, and internal short-circuit. SSEs are among the most promising electrolytes that can tackle the safety of commercial LIBs intrinsically, because of their mechanical strength and nonflammable nature. As shown in **Figure 6**, SSEs can be classified into three types: 1) solid inorganic electrolytes (SIEs), i.e., ceramics and ceramic glasses; 2) solid polymer electrolytes (SPEs); and 3) composite polymer electrolytes (CPEs).[125,126]

While solid-state batteries (SSBs) have shown considerable promise in the lab-scale, their realization is still challenging.[127–130] First, most SSEs perform well at HT (>60 °C), while RT and LT (<0 °C) operation remain a significant challenge. This is because, at RT, the transport of ions in solids is significantly slower (10^{-6} S cm^{-1}) than in liquids (10^{-2} S cm^{-1}).[19,20] Second, SSEs are characterized by high resistances at the solid/solid interfaces because of poor contacts and adverse interfacial reactions.[16,131,132] Third, the electrochemical window is often small because transition metals may lead to instability during

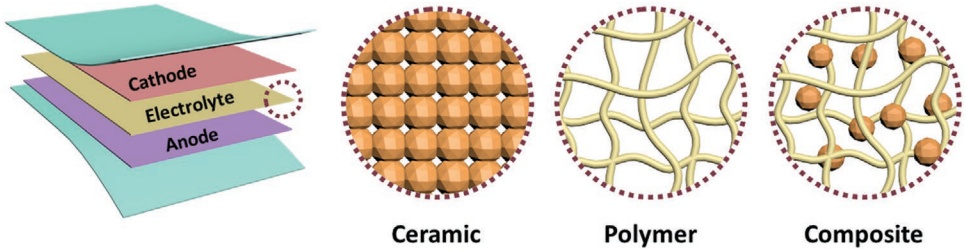

Figure 6. Types of solid-state electrolytes: ceramic, polymer, and composite.

redox reactions.[133,134] Fourth, most SIEs are brittle ceramics that need sintering. Therefore, it is difficult to make SIEs sufficiently thin. The high thickness not only increases the resistance but is also detrimental to the energy density.[135–138] In this section, we will review the SSEs that have been developed to operate for a broad range of temperatures.

4.1. Solid Inorganic Electrolytes

The SSBs composed of only SIEs are the ones typically regarded as true solid-state. Among SIEs, sulfides have the highest ionic conductivity. Notable examples include $Li_{10}GeP_2S_{12}$ (LGPS, 12 mS cm^{-1}),[139] $Li_{9.54}Si_{1.74}P_{1.44}S_{11.7}Cl_{0.3}$ (25 mS cm^{-1}),[140] Li_2S-P_2S_5 glass-ceramic or $Li_7P_3S_{11}$ (17 mS cm^{-1}),[141] $Li_{6.6}P_{0.4}Ge_{0.6}S_5I$ (18.4 mS cm^{-1}),[142] and $Li_{6.6}Si_{0.6}Sb_{0.4}S_5I$ (24 mS cm^{-1}).[143] Compared to oxides, sulfides typically are more conductive because of the lower the ionic activation barriers, the greater polarizability of their anions, and the softer lattice, see **Figure 7**.[144–149] Despite their high conductivity, sulfides have a narrow electrochemical window.[134,150,151]

Among oxide SIEs, garnet-type $Li_7La_3Zr_2O_{12}$ (LLZO) has shown considerable promise because it can be synthesized in air and is electrochemically stable with Li metal.[152–154] However, pristine LLZO has two different phases at standard conditions: i) a high-conductivity (10^{-4}–10^{-3} S cm^{-1}) cubic phase; ii) a low-conductivity (10^{-6} S cm^{-1}) tetragonal phase.[155] Aliovalent doping to make $Li_{7-3x}Al_xLa_3Zr_2O_{12}$,[156] $Li_{7-4x}Ge_xLa_3Zr_2O_{12}$,[157] $Li_{7-3x}Ga_xLa_3Zr_2O_{12}$,[158] or $Li_{7-x}La_3Zr_{2-x}Ta_xO_{12}$ (LLZTO)[159–161] has been employed as a strategy to stabilize the high-conductivity cubic phase.[162] A-site vacant perovskite-type $Li_{3x}La_{2/3-x}TiO_3$ (LLTO) is another promising oxide conductor because a variety of elements can be substituted in the A and B sites of LLTO (Figure 7c).[163] We should note that the conductivity of LLTO is rather low (10^{-5}–10^{-3} S cm^{-1}),[145,163] and the material is not stable against Li metal as Ti^{4+} can be reduced to Ti^{3+}.[163] However, these two issues can be resolved by replacing Ti^{4+} with less reducible cations such as Ta^{5+} and Hf^{4+} to form $Li_{3/8}Sr_{7/16}Hf_{1/4}Ta_{3/4}O_3$.[164] Interestingly, doping F in the O site to make $Li_{0.38}Sr_{0.44}Ta_{0.7}Hf_{0.3}O_{2.95}F_{0.05}$ (LSTHF)[165] yields a conductivity of 4.8×10^{-4} S cm^{-1} at RT. As a counterpart of the perovskite material, the antiperovskite Li_3OCl, where one O occupies the center of the octahedron to form the OLi_6 unit, see (Figure 7d), has also shown to be a fast Li conductor (Li conductivity $\approx 2 \times 10^{-3}$ S cm^{-1} at RT for $Li_3OCl_{0.5}Br_{0.5}$).[166] The derivatives of Li_3OCl, i.e., Li_2OHCl,[167] $Li_2(OH)_{0.9}F_{0.1}Cl$,[168] have been successfully used in SSBs. In particular, an SSB with Li_2OHCl demonstrated good stability and cyclability at 195 °C,[167] and an all-solid-state LFP/$Li_2(OH)_{0.9}F_{0.1}Cl$/Li battery has been operated at 65 °C for 40 cycles.[168] NASICON type materials, such as $Li_{1+x}Al_xTi_{2-x}(PO_4)_3$, and $Li_{1+x}Al_xGe_{2-x}(PO_4)_3$ (LAGP), with a general formula $Li_{4\pm x}Si_{1-x}X_xO_4$ (X = P, Al, or Ge) have also shown high conductivity (up to 10^{-2} S cm^{-1}) at RT.[169]

Typically, SIEs behave well at HT with the battery performance dropping as the temperature is lowered. This drop is mainly due to the decrease in ionic conductivity with

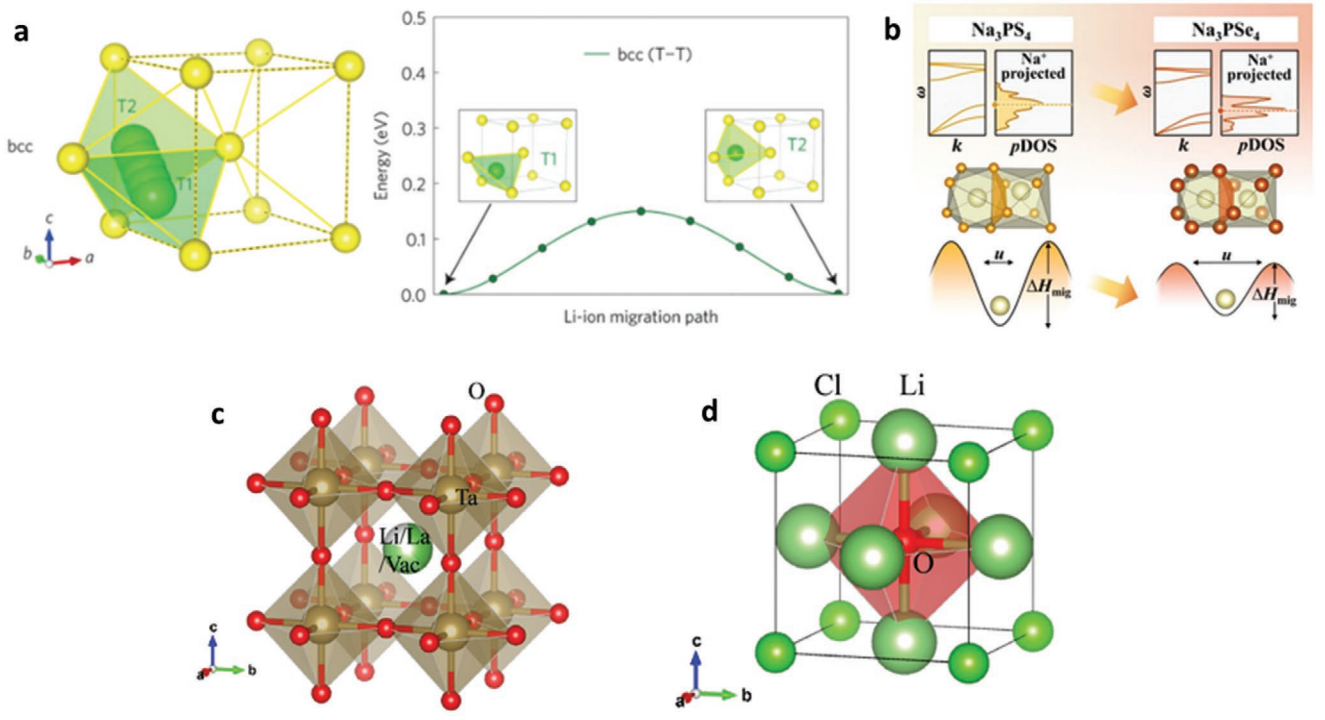

Figure 7. a) Ionic transport in bcc anion structure (left) and corresponding with migration energy profile (right). Reproduced with permission.[147] Copyright 2015, Springer Nature. b) Schematic illustration of the correlation between lattice dynamic softness and the energy landscape. Reproduced with permission.[148] Copyright 2018, American Chemical Society. Schematic illustration of crystal structures of c) $Li_{3x}La_{2/3-x}TiO_3$ (LLTO), and d) anti-perovskite Li_3OCl. In the perovskite structure, the octahedron is made up of TaO_6; however, in the anti-perovskite, the O atom occupies the center of the octahedron.

temperature following Arrhenius law. In order to enable the LT and RT performance for batteries, several strategies need to be introduced. While wetting the electrodes with LEs works well, the rigid solid/solid contacts between the SIEs and the electrodes yield large interfacial resistances, thereby lowering the ionic conductivities, rate capability, and energy density of the device. Several strategies have been developed to address this issue, including i) the introduction of lithiophilic or protective coatings;[170–172] ii) the fabrication of integrated SIEs/electrodes materials by blending or co-sintering;[173–175] iii) the design of porous SIE structures that increase the contact area between the electrode and electrolyte.[176,177] For example, Han et al.[170] minimized the interfacial impedance between the Li metal and the garnet-based solid electrolyte via atomic layer deposition (ALD). The garnet coated by ultrathin Al_2O_3 presented a much lower interfacial area-specific resistance than the pristine garnet at RT, i.e., 1 versus 1710 Ω cm^{-2}.

To extend the temperature range of SSBs, Kanno and co-workers[140] synthesized a chlorine-doped and silicon-based LGPS material of composition $Li_{9.54}Si_{1.74}P_{1.44}S_{11.7}Cl_{0.3}$ (**Figure 8**a–d). At RT, the conductivity was superionic, i.e., 25 mS cm^{-1}, a value twice as high as that of LGPS. The structure and Li density indicate that the Li transport in $Li_{9.54}Si_{1.74}P_{1.44}S_{11.7}Cl_{0.3}$ has two distinct routes, 1D along the *c* axis and 2D in the *ab* plane. The 1D pathway is typical in the materials within the LGPS family, while the 2D conduction mode contributes to increasing the ionic conductivity. The Kanno group also proposed another LGPS-based electrolyte ($Li_{9.6}P_3S_{12}$) for anode composite, which has high stability of ≈0 V versus Li. The LCO/$Li_{9.6}P_3S_{12}$/Li cell exhibited an initial CE of 90%. Such a high value suggests that most of the Li atoms from the cathode are deposited to the negative electrode as metal Li during charging. In contrast, the initial CE of the LCO/LGPS/Li and LCO/$Li_{9.54}Si_{1.74}P_{1.44}S_{11.7}Cl_{0.3}$/Li cells have been reported to be 61% and 39%, respectively. The corresponding SSBs exhibited minimal internal resistance and presented a superior performance between −30 and 100 °C, e.g., ≈130 mAh g^{-1} (0.05 C) at −30 °C and ≈130 mAh g^{-1} (2 C) at 100 °C (1 C = 0.667 mA cm^{-2}). Also, such SSBs had excellent rate capability (≈55 mAh g^{-1} at 1500 C) and cyclic stability (≈75 mAh g^{-1} over 500 cycles at 18 C) even at 100 °C.

The Jung group reported a scalable fabrication protocol for all-solid-state LIB electrodes by infiltrating LCO particles with a homogeneous SIE solution (e.g., Li_6PS_5Cl/ethanol).[178] LCO electrodes were first dip-coated in a Li_6PS_5Cl/ethanol solution. The subsequent removal of the solvent and heat treatment at 180 °C under a vacuum generated layer of solidified Li_6PS_5Cl. Finally, the Li_6PS_5Cl-infiltrated electrodes were densified by cold-pressing, providing improved contact between the phases. Li_6PS_5Cl possessed a conductivity of 0.19 mS cm^{-1} at RT. SSBs were assembled using LPSCl-infiltrated LCO (10 mg cm^{-2} of LCO) as the cathode and graphite (6 mg cm^{-2}) as the anode. These cells had a reversible capacity of 117 mAh g^{-1} and 65 mAh g^{-1} at 0.1 C and 30 °C and at 24 C and 100 °C, respectively.

Recently, Lee et al.[179] reported a high-performance all-solid-state LMB with a sulfide SIE (Li_6PS_5Cl), see Figure 8e–g. The thin Ag-C nanocomposite anode was able to regulate Li deposition effectively without the need for excess Li metal. The use of Ag improved the conductivity and lowered the nucleation energy of Li metal, and thus facilitated a uniform and dense Li metal layer. Warm isostatic pressing was also used to increase the density SSE film and improve the contact between electrode and electrolyte. The as-assembled NMC/Li_6PS_5Cl/Ag-C cell demonstrated a high specific capacity of ≈210 and ≈190 mAh g^{-1} at 60 and 25 °C (0.1 C), respectively. Even at LT, more than 80 and 150 mAh g^{-1} were delivered at −10 and 0 °C, respectively. A prototype pouch cell (0.6 Ah) thus prepared exhibited a high energy density (>900 Wh l^{-1}), stable CE over 99.8%, and long cycle life (1000 cycles).

All-solid-state LSBs with inorganic solid electrolytes may be able to simultaneously prevent the polysulfide shuttle effect and resolve the safety issues outlined in Section 2. However, due to the low ionic conductivity of solids and the unstable cathode/solid electrolyte interface, their rate and cycling performance need to improve.[180] Han et al.,[181] fabricated a novel class of all-solid-state LSBs based on the $Li_7P_3S_{11}$ glass-ceramic solid electrolyte ($\sigma = 2.0$ and 5.2×10^{-3} S cm^{-1} at RT and 80 °C, respectively) and a sulfur/carbon nanocomposite cathode (S@BP2000). The core-shell structure of S@BP2000 can improve the electrical conductivity, decrease the ohmic polarization, and accommodate the volume expansion of the electrode during cycling. The as-fabricated LSBs exhibited outstanding rate capacity (678.6 mAh g^{-1}, 4 C) and ultrastable cycling performance (capacity retention of ≈100% after 1200 cycles, 3 C) at RT. Both the specific capacity (1597.7 mAh g^{-1}, 0.2 C) and rate performance (1092.9 mAh g^{-1}, 8 C) improved at 80 °C because of the higher ionic conductivity.

For sulfide electrolytes, the main bottlenecks are the narrow electrochemical windows, low air stability, and the production of toxic H_2S gas if in contact with water. However, due to the softness of these materials, good electrolyte/electrode contacts can be achieved. For oxides, interfacial engineering can reduce the interfacial resistances typical of hard solid-solid contacts and enhance the wettability of Li. However, the brittleness of the pellet-type electrolytes is still a major limitation for application. In this regard, the research of SIEs should focus mainly on i) discovering fast Li conductors capable of operating over a wide range of temperatures; ii) reducing the interfacial resistance by improving the contacts that the electrolyte makes with the electrodes. The first challenge may be addressed by the ultrafast synthesis of ceramics,[182] a process that may also enable the rapid screening of promising SSEs. For the second challenge, the poor solid|solid contact may be alleviated by imposing an external pressure,[183] for example, warm isostatic pressing[179] during the assembly process.

4.2. Solid Polymer Electrolytes

SPEs have been extensively studied due to their good processability, flexibility, lightweight, cost-effectiveness, and good compatibility with electrodes. Generally, SPEs consist exclusively of polymers and Li salts without the addition of LEs. During the last three decades, various types of polymers are used in SPEs including PEO,[184–187] poly(vinylene carbonate) (PVCA),[188] poly(ethylene carbonate) (PEC),[189] poly(trimethylene carbonate) (PTMC),[190,191] perfluoropolyether (PFPE),[192] and poly(vinylidene difluoride) (PVDF).[193] Among them, PEO is the most commonly used polymer matrix. In PEO-based SPEs,

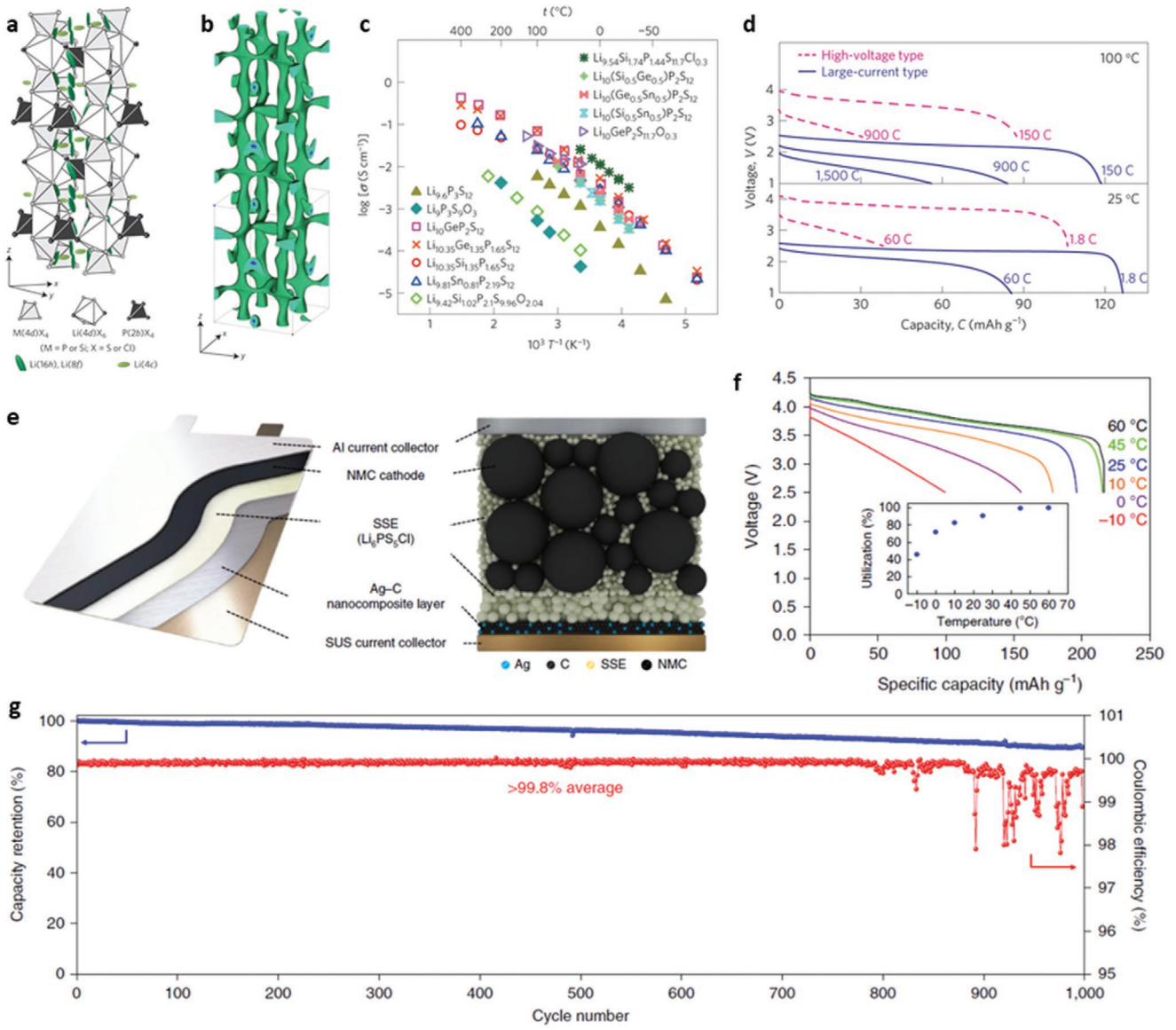

Figure 8. a) Crystal structure of $Li_{9.54}Si_{1.74}P_{1.44}S_{11.7}Cl_{0.3}$. The framework structure consists of 1D polyhedral chains (edge-sharing M(4*d*)X4 and Li(4*d*)X6) connected by P(2*b*)X4 tetrahedra. Conducting lithium is located on the interstitial site of Li(16*h*), Li(8*f*) and Li(4*c*). b) Nuclear distribution of Li atoms in $Li_{9.54}Si_{1.74}P_{1.44}S_{11.7}Cl_{0.3}$ at 25 °C, calculated using the maximum entropy method at the iso-surface level of −0.06 fm Å^{-3}. c) Arrhenius conductivity plots for the LGPS family and $Li_{9.6}P_3S_{12}$ and $Li_{9.54}Si_{1.74}P_{1.44}S_{11.7}Cl_{0.3}$. d) Extraction of discharge curves for the prepared all-solid-state cells. The rate *n*C corresponds to the full charge and discharge of the theoretical capacity of 0.667 mAh in 1/*n* h. Reproduced with permission.[140] Copyright 2016, Springer Nature. e) Schematic of an all SSB composed of a NMC cathode with a high areal capacity (>6.8 mAh cm^{-2}), SSE and a Ag-C nanocomposite anode layer that does not require excess Li. Al and stainless steel foil were used as current collectors for the cathode and anode, respectively. f) Discharge capacities were monitored under 0.1 C/0.1 C charge/discharge conditions as the discharging temperature was varied from 60 to −10 °C. The charging temperature was fixed at 60 °C. g) Cycling performance and CE of the Ag-C|SSE|NMC prototype pouch cell (0.6 Ah) are plotted against the cycle numbers. A constant current mode with the charge/discharge rate of 0.5 C/0.5 C was applied (voltage window, 2.5–4.25 V vs Li^+/Li at 60 °C). The areal capacity loading of the NMC cathode was 6.8 mAh cm^{-2} (1.0 C = 6.8 mA cm^{-2}). Reproduced with permission.[179] Copyright 2020, Springer Nature.

Li-ions are dissociated from Li salts, coordinated with the electron-donor groups (−CH_2CH_2O−) in the polymer chain. Then, Li-ions transport from one coordinating site to another. It is generally believed that the ionic conduction in PEO-based SPEs occurs in the amorphous part of the PEO matrix, while the crystalline part delivers limited ion transport.[194] Since the PEO chain is mainly crystalline at RT, the PEO-based SPEs normally exhibit low ionic conductivities (<10^{-6} cm^{-1}).[195] Therefore, the SSBs with PEO-based SPEs require higher working temperatures, typically >60 °C. While SPEs are regarded as a safer alternative to conventional LEs for HT electrochemistry, working at HT hampers their mechanical properties. Such limited ionic conductivity greatly restricts the application of PEO-based SPEs.

An ideal polymer matrix for SPEs should be endowed with the following properties: i) dissolubility of the salt to form

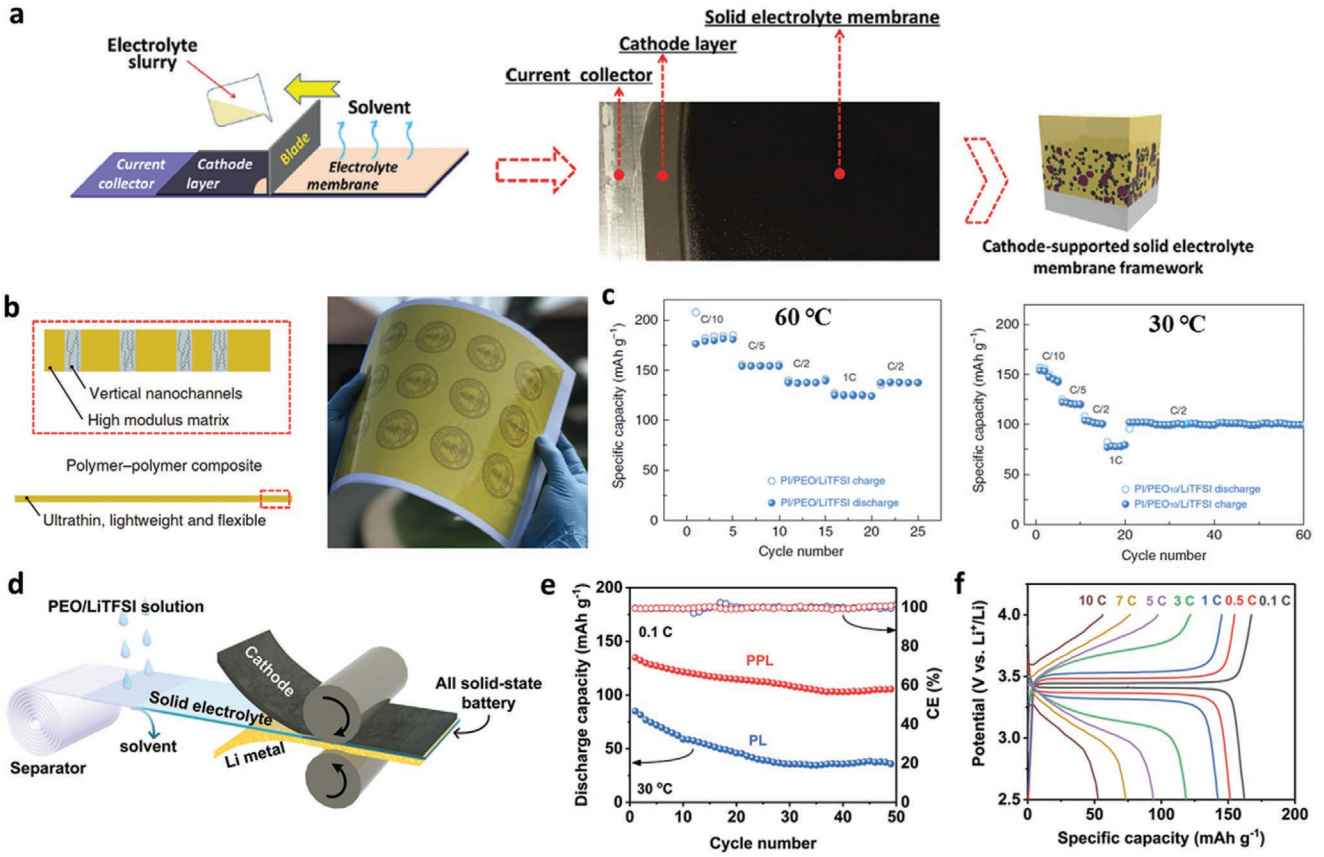

Figure 9. a) Schematic illustrating the preparation of a cathode-supported solid electrolyte membrane by tape casting; the electrolyte slurry was tape cast onto the dry cathode tape showing a compact structure after drying. Reproduced with permission.[198] Copyright 2019, Royal Society of Chemistry. b) Schematic showing the design principles of a polymer-polymer composite solid-state electrolyte and photo image of a large-scale porous PI film. c) Cycling performance of a LFP/PI/PEO/LiTFSI/Li cell at different charging rates with the cycling being carried out at 60 and 30 °C. Reproduced with permission.[185] Copyright 2019, Springer Nature. d) Schematic illustration of the fabrication process. e) Cycling performance of all-solid-state LIBs with PPL electrolytes at 30 °C and 0.1 C. f) Voltage profiles of LFP/PPL/Li battery at various current densities (60 °C). Reproduced with permission.[197] Copyright 2019, John Wiley and Sons.

polymer-salt complexes, and capability to facilitate cationic hopping from one coordinating group to another; ii) flexibility and mechanical strength to allow for simple processing; iii) large electrochemical window (>4.5 V vs Li^+/Li) to prevent oxidation; iv) high ionic conductivities (>1 × 10^{-4} S cm^{-2} at RT) and ion transference numbers (>0.6); v) chemical and thermal stability to enlarge the temperature window and ensures the safety of the SPE-based SSBs. In recent years, various strategies have been utilized to improve the ionic conductivity and extend the operating temperature of SPEs, including employing novel structural polymers, optimizing the Li salts, and introducing organic plasticizers.

For SSEs, the ionic conductance, a function of the thickness, is more directly related to the performance and energy density of SSBs than the ionic conductivity.[196,197] The ionic conductance, G, is given by

$$G = \sigma \frac{A}{l} \quad (1)$$

where, A, and l denote the ionic conductivity, surface area, and thickness of the SSEs, respectively. Therefore, lowering the thickness of SPEs improves the ionic conductance and decreases the Ohmic resistance, thereby enhancing battery performance. For this purpose, researchers proposed various strategies to minimize the thickness of SPEs. PEO possesses low MP (65 °C), good solubility, and film-forming ability. Therefore, this can be used to make thin SPE films with methods as diverse as hot-pressing, solution casting, and hot-melting infiltration. For example, as shown in **Figure 9**a, the Wang group[198] prepared a novel cathode-supported SSE membrane using a simple bilayer tape-casting technique. Specifically, a cathode electrode tape was first fabricated by casting. Then, the PEO-based electrolyte slurry was directly placed onto the cathode to fabricate an electrolyte-cathode assembly. The thicknesses of the cathode layer and the solid electrolyte layer were about 11.2 and 9.5 µm, respectively. This design optimized the interfacial contact between the cathode and the electrolyte by strengthening the interfacial adhesion and filling the cathode's pores. When operated at 0.1 C, the LFP/Li cathode-supported all-solid-state LIBs could deliver discharge capacities of 125 and 167 mAh g^{-1} at 30 and 50 °C, respectively.

The Cui group[185] reported the design of a safe SPE composed of a flexible, nonflammable, and porous polyimide (PI) host, and PEO/LiTFSI fillers. As shown in Figure 9b, the

PI matrix was 8.6 µm thick and had vertically aligned nanochannels. The ionic conductivity (2.3×10^{-4} S cm^{-1} at 30 °C) was significantly higher than that of a PEO/LiTFSI thin film (5.4×10^{-5} S cm^{-1}). The MD simulations indicated that the Li-ion diffusivity was faster along the channel ($D = 1.3 \times 10^{-8}$ cm^2 s^{-1}) than in the random system ($D = 5.7 \times 10^{-9}$ cm^2 s^{-1}). Also, the PI material exhibited a much larger modulus than PEO/LiTFSI film, i.e., 850 versus 0.1 MPa. These properties effectively suppressed the growth of dendrites and prevented the fabricated Li/SPE/Li symmetric cells from short-circuiting during the 1000 h cycling test. The all-solid-state LFP/SPE/Li cell fabricated with the PI/PEO/LiTFSI SPE was able to undergo 200 cycles at 0.2 C and 60 °C (Figure 9c). At lower temperatures (e.g., 30 and 40 °C), such LIBs still had a capacity larger than 120 mAh g^{-1}. Nail penetration and cutting tests were also carried out on LFP/SPE/Li pouch cells. After these tests, the LFP/SPE/Li pouch cell could still power an LED bulb.

Similarly, Wu et al.[197] recently developed an ultrathin SPE (7.5 µm), denoted as PPL, by infiltrating PEO/LiTFSI into a 5 µm thick polyethylene separator (Figure 9d). The ionic conductivities of PPL were 3.68×10^{-5} and 1.54×10^{-4} S cm^{-1} at 30 and 60 °C, respectively, slightly lower than those of PEO/LiTFSI SPEs (5.01×10^{-5} S cm^{-1} at 30 °C and 4.20×10^{-4} S cm^{-1} at 60 °C). The transport activation energies of the PPL and PEO/LiTFSI SPEs were estimated to be 0.32 and 0.45 eV, respectively. The ultrathin PPL shortened the Li diffusion pathway, thereby providing a sufficiently low resistance that allowed the batteries to operate at RT. As shown in Figure 9e,f, all-solid-state LFP/PPL/Li batteries delivered an initial discharge capacity of 135 mAh g^{-1} at 30 °C and 0.1 C, and an excellent rate performance (≈90 mAh g^{-1}) up to 5 C at 60 °C. At an increased LFP loading of 7 mg cm^{-2}, the PPL-based batteries had a reversible capacity of 135 mAh g^{-1} at 0.1 C and 60 °C. Corresponding pouch cells were assembled and tested. Even if folded at a 45 or 135° angle, a reversible discharge capacity of ≈120 mAh g^{-1} (0.1 C, 60 °C) could be obtained. Also, an LED could be lit even after nail penetration and cutting in half.

The PEO-derived acrylates were also employed to synthesize network structural SPEs. Such SPEs can be simply obtained by an in situ crosslinking reaction, e.g., UV and/or thermal initiated polymerization.[199] For example, Xu and co-workers[200] prepared a novel SPE with high ionic conductivity using a solvent-free photopolymerization method (**Figure 10**a,b). UV polymerization was used to turn a mixture of liquid poly(ethylene glycol) methyl ether methacrylate (PEGDMA) monomer and LiTFSI into a solid. The comb-like polymer chain structures were beneficial to Li^+ transport because of their large free moving volume and rotation space. Therefore, this SPE had an ionic conductivity of 2.35×10^{-4} S cm^{-1} at RT. The corresponding $LiMn_{0.8}Fe_{0.2}PO_4$/SPE-PEGDMA$_{480}$/Li (LMFP/SPE-PEGDMA$_{480}$/Li) batteries delivered an excellent capacity of 124.6 mAh g^{-1} (0.1 C, 200 cycles) and 154.7 mAh g^{-1} (0.5 C, 450 cycles) at 25 and 60 °C, respectively. Also, the LMFP/SPE/Li pouch cell could still power an LED after folding and cutting.

Due to the low dielectric constant of PEO, the partial dissociation of Li salts will lead to the aggregation of ions, which reduces the ionic conductivity of PEO-based SPEs. Carbonates are generally employed as commercial LEs with the great advantage of high dielectric constant and good salt dissociation. Introducing carbonate-based groups (—O—(C=O)—O—) into the polymer is an effective strategy to design high-performance SPEs.[188,201] For example, Zhang et al.[202] proposed a safe poly(propylene carbonate) (PPC)-based SPEs (CPPC-SPE) for LIBs operating over a wide range of temperatures (5–120 °C). At 20 °C, the CPPC-SPE had a higher ionic conductivity that PEO-SPE, i.e., 3.0×10^{-4} versus 2.1×10^{-6} S cm^{-1}. The high degree of crystallinity of PEO significantly hampered the transport of

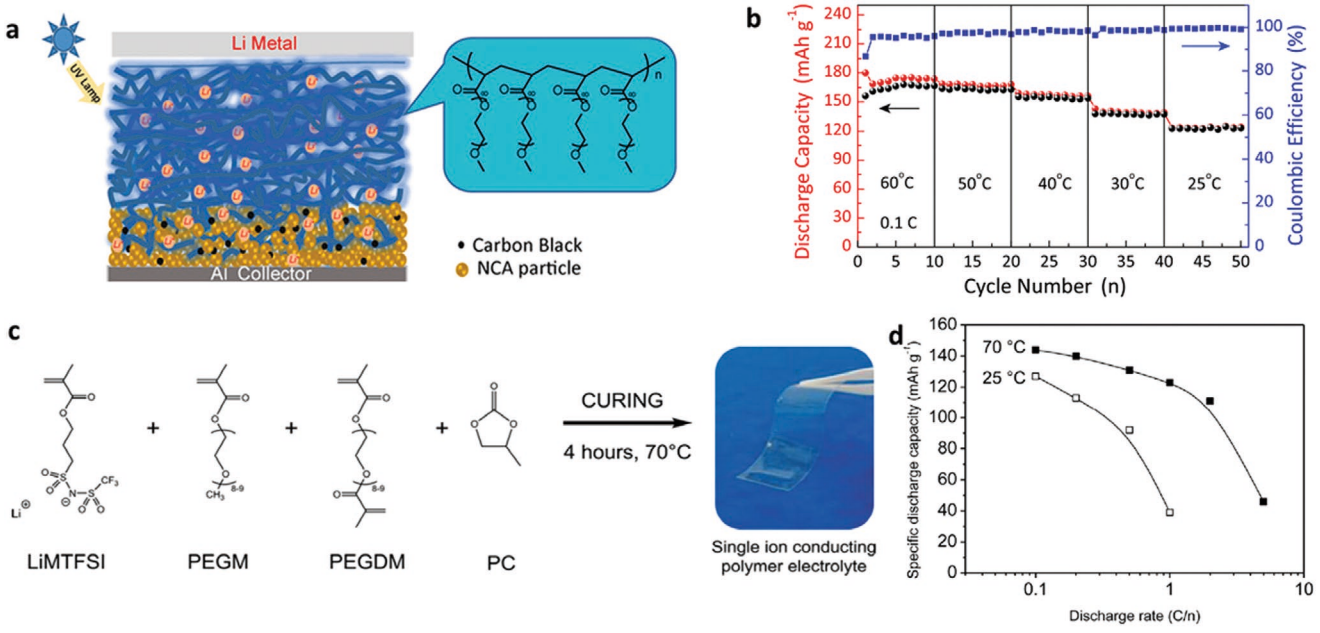

Figure 10. a) The process used for polymer electrolyte fabrication and battery assembly. b) Cycle performance of LMFP/SPE-PEGDMA$_{480}$/Li battery at different temperatures. Reproduced with permission.[200] Copyright 2019, Elsevier. c) General pathway for the preparation of SIPE films. d) The discharge capacity of the cells at 25 and 70 °C. Reproduced with permission.[208] Copyright 2016, American Chemical Society.

Li ions, resulting in low ionic conductivity at ambient temperature.[203] In contrast, the transient cross-linking complex, which was formed by the interaction of Li and the C=O groups of PPC, enabled a faster migration path for Li^+. Also, the amorphous structure of the PPC-SPE increased the mobility of Li in the polymer chains and lowered the transport barrier. Moreover, differential scanning calorimetry (DSC) tests suggested that the CPPC-SPE does not melt below 120 °C. As a result, LIBs with CPPC-SPE could be cycled 1000 times at 20 °C (≈100 mAh g^{-1}, 0.5 C) and 500 times at 120 °C (≈95 mAh g^{-1}, 3 C), respectively. Moreover, the pouch cell could successfully power an LED bulb even if a corner was cut.

The addition of ion-conducting plasticizers has proven to be a viable strategy for enhancing the dissolution of Li salts and ionic conductivity of SPEs. Typically, the plasticizers can be divided into three classes: i) nitriles (e.g., succinonitrile),[204–207] ii) carbonates/ethers (e.g., PC),[208,209] and iii) ILs.[96,210] The employment of thermally stable plasticizers can significantly improve the performance of SPEs both at RT and HT. Zhu and co-workers[211] designed SPEs leveraging the ternary phase diagrams of a combination of crosslinked poly(ethyleneglycol) diacrylate (PEGDA), Li salt, and plasticizer. Samples with different concentrations of crosslinked PEGDA, glutaronitrile (GN), and Li salt were used to make a highly conducting (σ = 1.0 mS cm^{-1} at 30 °C and 4.9 mS cm^{-1} at 100 °C) and free-standing dual-salt SPE (DS-SPE). The synergy of LiTFSI and LiBOB endowed the DS-SPE with outstanding electrochemical stability. While LiBOB protected the Al collector, which can be corroded by LiTFSI, LiTFSI mitigated the reaction of LiBOB with the Li metal electrode. The LFP/DS-SPE/Li cells exhibited an outstanding capacity of ≈118 mAh g^{-1} (0.2 C) and an average CE of 99.99% over 370 cycles at 30 °C. At 75 °C, the initial specific capacity increased to 147 mAh g^{-1}, with a 76% capacity retention after 100 cycles.

PILs have a unique chemical structure, where IL species are covalently bonded with the polymer backbones. Therefore, PILs possess the advantage of both ILs and polymers, including nonflammability, high thermal and electrochemical stability, good mechanical performance, and processability.[51,96] Li et al.[210] developed a sort of SPE with a broad range of operating temperatures (25–80 °C). The pyrrolidinium-based PIL was employed as a polymer matrix, and *N*-ethyl-*N*-methylpyrrolidinium bis(fluorosulfonyl)imide ($P_{12}FSI$) was added as plastic. The PIL inherited several characteristics of ILs, including an excellent film-forming ability, a high MP (205 °C), an increased ionic conductivity, and improved electrolyte/electrode contacts. In particular, the corresponding SPEs exhibited ionic conductivities above 10^{-4} S cm^{-1} at 25 °C. The LFP/SPE/Li cells with these SPEs presented high discharge capacities and excellent cyclic stability, e.g., 150 and 160 mAh g^{-1} for 150 cycles (0.2 C) at 25 and 80 °C, respectively.

Polymer chemistry can be leveraged to design polymer matrices with functional units.[8,212,213] In this context, single-ion conducting polymers (e.g., poly(styrene trifluoromethanesulphonylimide of lithium) and poly(lithium 1-(3-(methacryloyloxy) propylsulfonyl)-1-(trifluoromethylsulfonyl)imide)) have been developed to immobilize anions (e.g., methacrylate and trifluoromethanesulphonylimide) by covalently tethering them to the polymer backbone, consequently increasing t_{Li^+}.[208,214–218] This strategy not only allows the Li ions to be the only mobile species but also the anions contribute to a uniform distribution of Li ions and a dendrite-free Li deposition.[219] However, such single-ion conductors are typically characterized by poor ionic conductivities at RT (<10^{-7} S cm^{-1}). For instance, Bouchet et al.[215] developed anionic triblock copolymers for all-solid-state LMBs capable of delivering ≈145 mAh g^{-1} at C/4 and 80 °C. Gerbaldi and co-workers[208] designed a SIPE possessing a t_{Li^+} nearing 1 and ionic conductivity of 1.2×10^{-4} S cm^{-1} at RT, see Figure 10c. The SIPE was prepared using an in situ radical copolymerization of lithium sulfonamide methacrylic monomer with poly(ethylene glycol) methyl ether methacrylate (PEGM) and poly(ethylene glycol) methyl ether dimethacrylate (PEGDM) and the presence of PC as a plasticizer. Compared to conventional electrolytes, the SIPE's anions were covalently bonded to the polymer network and the ionic current was mainly carried by Li^+. Thus, the SIPE provided transference number values as high as 0.86 ± 0.02 and 0.90 ± 0.02 at 25 and 70 °C, respectively. As shown in Figure 10d, the LFP/SIPE/Li cells delivered high capacities of 126 and 143 mAh g^{-1} (0.1 C) at 25 and 70 °C, respectively.

The properties of recently reported SPEs characterized by a wide temperature window are summarized in **Table 1**. Despite the significant progress in the SPE area, more efforts are needed to enhance the performance and broaden the temperature window of SPEs. First, SPEs, especially if operated at RT, is characterized by low ionic conductivities. Novel polymer materials with high ionic conductivity should be explored. Polymer engineering strategies such as copolymerization, cross-linking, and grafting, can be used to suppress the crystallization of polymer matrices and improve ionic conductivity. Second, increasing the Li-ion transference number is also critical because it can simultaneously reduce the polarization resistance and suppress Li dendrite growth. Third, the SPEs' electrochemical and thermal stabilities need to be enhanced to increase their lifespan. To improve safety, it is also necessary to design SPEs with additional functionalities, such as self-healing, overheating protection, and self-extinguishing feature.

4.3. Composite Polymer Electrolytes

The CPEs typically consist of soft polymers and rigid inorganic fillers. Generally, the introduction of inorganic fillers into the SPEs can significantly enhance the mechanical strength and increase the RT ionic conductivity.[220–227] The incorporated inorganic fillers can be divided into two categories, i.e., non-conductive fillers (e.g., Al_2O_3, TiO_2, ZrO_2, and SiO_2) and ionic conductive fillers (e.g., LLZO, LLZTO, LGPS, and LAGP). The ionic conductivity increases mainly due to the hinder reduction of the crystallization and the increment of the segmental motion of polymer matrices with the presence of stiff nanoparticles.[228,229] Further, the fillers can enhance thermal stability and delay the generation of Li dendrites.[230] Concomitantly, the soft and flexible SPE matrix improves the interfacial compatibility between electrodes and electrolytes. If fast ionic conductors are added into a composite solid electrolyte, the composite can also benefit from the ionic conductivity of the SIEs. Various groups have shown that the electrochemical performance of CPEs can be significantly promoted by including Li^+-stuffed ionic-conducting fillers in PEO,[229,231–234] PPC,[235]

Table 1. Summary of reported wide-temperature operable SPEs for LIBs.

Electrolyte	Ionic conductivity [mS cm^{-1}]	Capacity [mAh g^{-1}]	Operating temperature [°C]	Current density [C]	Cathode	Ref.
PI/PEO/LiTFSI	0.23, 30 °C	100–138	30–60	0.5	LFP	[185]
CPPC-SPE	0.3, 20 °C; 1.4, 120 °C	103–138.7	20–120	1	LFP	[202]
PPAL	–	125–167	30–50	0.1	LFP	[198]
MSTP-PE	0.36, 25 °C; 3.53, 80 °C	126–154	5–60	0.1	LFP	[209]
Cellulose/PVCA-LiDFOB	0.0223, 25 °C; 0.0982, 50 °C	97–123	25–50	0.1	LCO	[188]
SPE-$PEGDMA_{480}$	0.235, 25 °C	124–168.7	25–60	0.1	LMFP	[200]
P(V-B)	0.911, 25 °C	≈55–70	10–60	0.5	LFP	[201]
[50/50]/20 SPE	0.154, 25 °C; 1.26, 80 °C	150–165	25–80	0.2	LFP	[210]
SPE-1	0.05, 25 °C; 0.285, 60 °C	≈100–163.9	25–60	0.1	LFP	[199]
DS-SPE	0.84, 30 °C; 4.9, 100 °C	≈123–147	30–75	0.2	LFP	[211]
PPL	0.0368, 30 °C; 0.154, 60 °C	135–160	30–60	0.1	LFP	[197]
SPH15	0.12, 30 °C; 0.34, 60 °C	84–140	10–60	0.5	LFP	[186]
SIPE3	0.12, 25 °C	126–143	25–70	0.1	LFP	[208]

polyacrylonitrile (PAN),[236] PVDF,[237–239] and PVDF-HFP[37,240] polymer matrices.

According to the content of the ceramic fillers, the CPEs can be divided into two types, i.e., ceramic-rich (>50 wt%) CPEs (polymer-in-ceramic) and polymer predominant CPEs (ceramic-in-polymer). Increasing ceramic fillers improve the mechanical strength and safety (especially at HT), but the high loading can lead to aggregation, and result in phase separation, lower ion migration, and poor miscibility between the polymer and filler.[237] Moreover, a high ceramic content embrittles the CPEs, making it difficult to make a uniform and free-standing membrane. Therefore, the design of CPEs requires performance trade-off.

Hot-pressing is an efficient, scalable, and environmental-friendly technology for CPEs fabrication that does not require a solvent. For example, the Gerbaldi group[233] fabricated a CPE by hot pressing the solid mixture of PEO-LiTFSI and LAGP. Their best CPE contained 60 wt% of LAGP and had an ionic conductivity of 1.6×10^{-5} S cm^{-1} at 20 °C, one order of magnitude higher than that of LAGP-free samples. The incorporation of LAGP improved thermal stability and the electrochemical performance across a wide range of temperatures (25–80 °C), while the LAGP-free electrolytes could not work below the PEO melting temperature (55 °C). Goodenough and co-workers[229] developed two classes of CPEs integrated with LLZTO, PEO, and LiTFSI via a hot-pressing technology, including ceramic-in-polymer and polymer-in-ceramic electrolyte systems (**Figure 11**a). The soft PEO polymer matrix provided a large contact area enabling interfacial compatibility. LLZTO contributed to enhancing Li^+ conductivity. Rigid LLZTO particles integrated with the PEO chain segments provided a mechanically robust framework against the growth of Li dendrites. These two CPEs demonstrated strikingly different characteristics. The ceramic-in-polymer electrolyte showed remarkable flexibility, while the polymer-in-ceramic electrolyte possessed better mechanical robustness and yielded higher safety. The ceramic-in-polymer with 10 wt% LLZTO filler obtained the highest ionic conductivity up to 1.17×10^{-4} S cm^{-1} at 30 °C and 1.58×10^{-3} S cm^{-1} at 80 °C. Both values were higher than those obtained with a PEO-based electrolyte. Both ceramic-in-polymer and polymer-in-ceramic electrolytes were successfully used to make solid-state LFP/CPE/Li batteries, demonstrating excellent cycling stability, discharge capacity, and rate performance, i.e., 119.2 to 151.4 mAh g^{-1} at 0.2 C within a temperature change from 25 to 75 °C for the ceramic-in-polymer electrolytes and 127 mAh g^{-1} (0.2 C) with 100% CE over 50 cycles at 55 °C for the polymer-in-ceramic electrolytes. Generally, PEO electrolytes can react with Li metal and generate a Li_2O passivation film, which increases the electrode/electrolyte interfacial resistance. The addition of LLZTO particles reduces the contact between the Li metal and PEO matrix and thus impedes the passivation reactions. As a result, the CPE with 85 wt% of LLZTO demonstrated good compatibility with the Li-metal anode and delivered outstanding cyclic stability over 680 h for symmetric cell (55 °C).

The Cui group[235] developed a free-standing CPE with PPC and 5 wt% of LLZTO, which hereon we will indicate as PPCL-SPE, for flexible all-solid-state LIBs operating between 0 to 160 °C, see Figure 11b. The introduction of LLZTO nanoparticles could not only decrease the crystallinity but also add free volume for the PPC, thereby favoring the movement of the polymer chain segments and the migration of Li ions. Moreover, the LLZTO was shown to promote the dissociation of Li salts thanks to the interaction between LiTFSI and the surface of the LLZTO nanoparticles. This interaction resulted in a higher free Li^+ concentration in the polymer matrix and the formation of

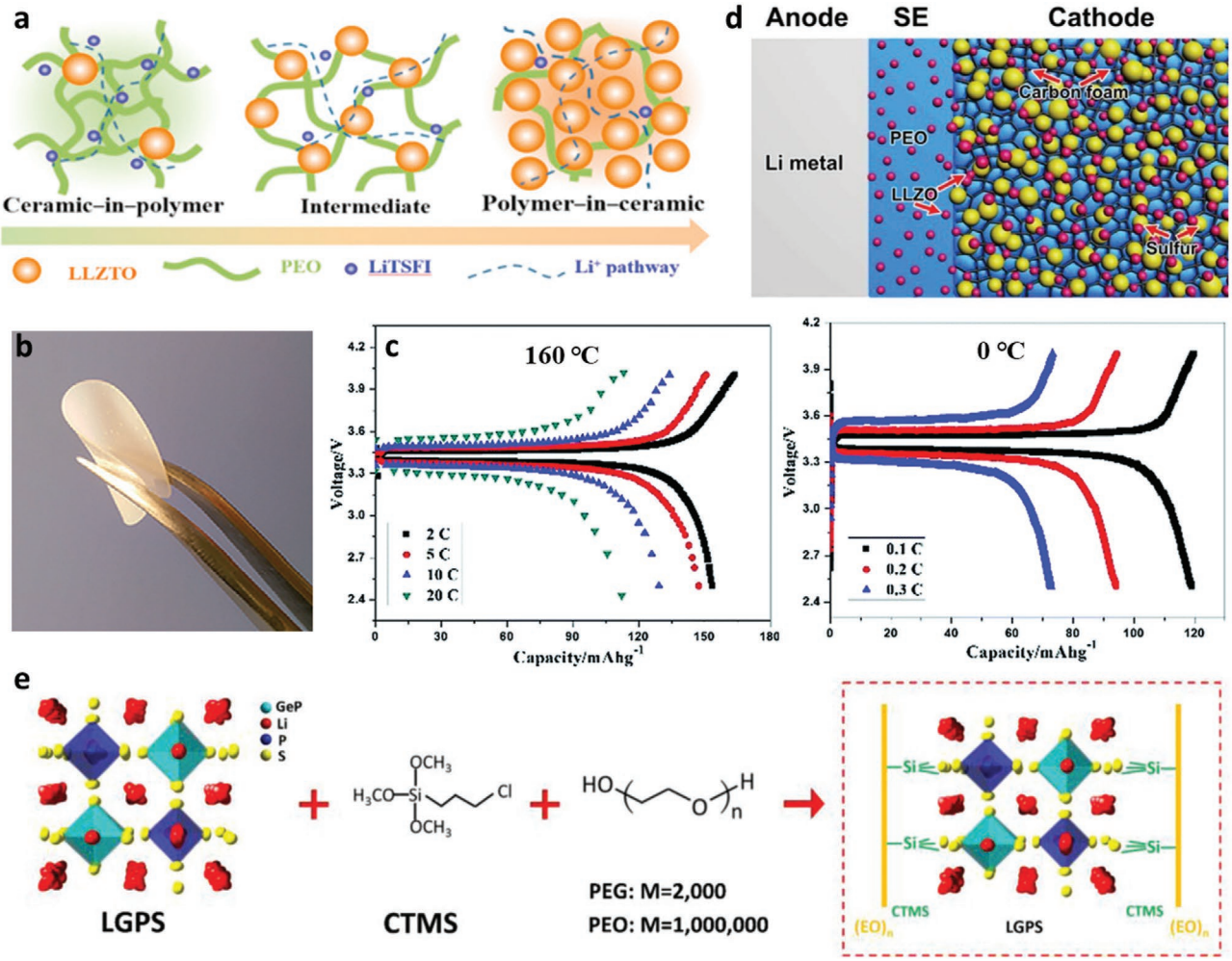

Figure 11. a) Schematic illustration for PEO-LLZTO: "ceramic-in-polymer," "intermediate," and "polymer-in-ceramic." Reproduced with permission.[229] Copyright 2018, Elsevier. b) Optical photograph of flexible PPCL-SPE. c) Typical charge/discharge curves of solid-state LFP/PPCL-SPE/Li battery at 160 and 0 °C. Reproduced with permission.[235] Copyright 2017, Royal Society of Chemistry. d) Schematic illustration of an all-solid-state LSB based on LLZO nanostructures. The construction of the S cathode using an LLZO@C matrix and PEO binders aims at reducing the interfacial resistance. The carbon matrix is an LLZO particle decorated porous foam network. S is uniformly dispersed in the porous carbon matrix. The LLZO-PEO-$LiClO_4$ electrolyte is cast onto the composite cathode directly. Reproduced with permission.[241] Copyright 2017, American Chemical Society. e) Schematic illustration of the as prepared HSE structure. Reproduced with permission.[244] Copyright 2020, John Wiley and Sons.

ionically conductive paths along with the PPC/LLZTO interfaces. The as-obtained PPCL-SPE displayed a high ionic conductivity ($\sigma = 5.2 \times 10^{-4}$ S cm^{-1}) at 20 °C, a wide electrochemical window (4.6 V vs Li^+/Li), and a high Li^+ transference number ($t^+ = 0.75$). Furthermore, the solid LFP/PPCL-SPE/Li battery delivered an excellent rate capability of ≈90 mAh g^{-1} at 5 C, and superior cycling stability (200 cycles at 1 C) with 95% retention at RT. Also, as reported in Figure 11c, the battery still delivered a satisfactory charge/discharge performance between 0 and 160 °C.

Cui and co-workers[241] developed a class of all-solid-state CPEs based on Al^{3+}/Nb^{5+}-codoped cubic LLZO and PEO, see Figure 11d, for use in LSBs. The introduction of Al was beneficial for the stabilization of cubic LLZO at RT. Adding Nb effectively enhanced the ion conductivity because of a higher concentration of Li vacancies. The sulfur cathode was a composite consisting of LLZO-decorated porous carbon foam (LLZO@C), sulfur, and PEO that was directly cast on the composite cathode to allow a low electrolyte/electrode interfacial resistance. This combination enabled both ionic and electronic conductive paths. Consequently, the resulting LSBs exhibited an impressive specific capacity of ≈800 mAh g^{-1} over 200 cycles with 0.05 mA cm^{-2} at 37 °C, and a high capacity of 1210 and 1556 mAh g^{-1} at 50 and 70 °C, respectively.

In conclusion, the CPEs synergistically combine the beneficial properties of both SIEs (high ionic conductivity and strength) and SPEs (good interfacial properties and flexibility). Therefore, CPEs have very promising prospects for the future development of all SSBs. The main dilemma of CPEs is related to the low chemical and mechanical compatibilities between ceramic and polymeric phases. Mechanical mixing or solution mixing is indeed a convenient and cost-effective method. However, the poor interfacial compatibility between fillers and polymer may lead to a failure in making an effective ion conductive network. Also, the local aggregation of fillers/polymer hinders the ion

migration and thus decreases the ionic conductivity of CPEs. To solve those issues, surface modification of the fillers may improve the chemical compatibility between filler and polymer, thereby increasing the ionic conductivity via the Li^+ domain-diffusion effect.[242] Moreover, chemical crosslinking is an effective strategy to prepare network structural materials. For example, Yan et al.[243] decorated acrylate functional groups on the surface of 1D $Li_{6.28}La_3Al_{0.24}Zr_2O_{12}$ (LLAZO). Then, the modified LLAZO was covalently cross-linked with the PEGDA matrix via thermal-initiated polymerization. Such a strategy significantly improved the distribution of inorganic fillers and reduced the activation energy of Li^+ conduction between the filler and polymer. Recently, Zhang and co-workers[244] made a flexible CPEs using an in situ coupling reaction (Figure 11e), that bonded silane was with both PEG and LGPS. Such a linkage guaranteed the fast ionic transportation between the two. The as-prepared membrane had an ionic conductivity of 9.83×10^{-4} S cm^{-1} at RT and a high Li^+ transference number of 0.68. Furthermore, the growth of Li dendrites was suppressed: a symmetric Li cell operated at a current density of 2 mA cm^{-2} could cycle stably over 6700 h at RT.

5. Computational for the Design and Mechanistic Understanding of Electrolytes

Atomistic modeling is establishing itself as a useful tool for understanding and designing electrolyte materials. Commonly used methods include first-principles calculations (e.g., density functional theory (DFT)), and MD (e.g., classical and ab initio MD simulations (AIMD)).[245,246] We will review below how atomistic simulations have been used to model electrolytes. We will also show how continuum modeling and artificial intelligence (AI) could be used to design new battery electrolytes.

5.1. Ionic Diffusional Properties

A key requirement of a battery electrolyte is a high ionic conductivity. The conductivity, σ, can be obtained from[247,248]

$$\sigma = \frac{q^2 c}{k_B T} D \tag{2}$$

where q and c are the charge and concentration of the mobile species, respectively, k_B is the Boltzmann constant, T is the temperature, and D is the self-diffusion coefficient. In principle, the higher the temperature, the faster is the transport of mobile ions. To enable the batteries' operation at or below RT, the conductivity should not drop rapidly, i.e., the electrolyte should have a low enough activation energy, E_a. The relationship between σ and T follows the Arrhenius equation

$$\sigma T \sim \exp\left(-\frac{E_a}{k_B T}\right) \tag{3}$$

For LEs, the ionic conductivity is dependent on several properties, e.g., solvent dielectric permittivity, solvent viscosity, temperature, and salt concentration.[249] To obtain a sufficiently high cationic conductivity, the solvent should have: i) a high dielectric permittivity so that cations can be dissociated from the anionic framework; and ii) a low viscosity. However, a single solvent, which meets the above requirements simultaneously, has not been identified yet. Consequently, solvents with high dielectric permittivity (e.g., EC), and low viscosity (e.g., DMC and DEC), are typically mixed into the electrolytes of conventional Li batteries.[249] Borodin and co-workers studied using MD simulations a mixed solvent electrolyte system combining EC and DMC with a $LiPF_6$ salt. These authors found an increase in the free ion concentration and a decrease in ion and solvent diffusion coefficients with the EC concentration.[250,251] As a result of this tradeoff, the maximum Li conductivity was obtained with a 1:1 EC and DMC solution.

Although choosing a solvent with a high dielectric permittivity can significantly improve the Li conductivity, it also brings challenges. First, the Li-ion transference number is significantly reduced due to the strong binding of the Li^+ to the solvents.[252] Second, the freezing temperature increases because of the enhanced dipole–dipole attraction among more polar molecules. The combination of these two factors hampers the LT conductivity of the electrolytes.[68] Therefore, to improve the conductivity, the affinity between solvents and Li^+ ions should be adjusted. Wang and co-workers designed a new electrolyte by dissolving fluorinated compounds (LiFSI-FEC/FEMC or lithium bis(pentafluoroethanesulfonyl)imide (LiBETI)-FEC/DEC) into highly fluorinated nonpolar solvents. This combination was able to break the strong interaction between the highly polar solvent molecules, thus widening the liquid-phase stability range.[68] MD simulations demonstrated that the addition of nonpolar solvents could enhance the Li-ion transference number by decreasing the coordinated solvent molecules with Li^+.[68] Experimental results confirmed that doing so led to a high ionic conductivity (>10^{-2} mS cm^{-1} at −80 °C) at a temperature range between −125 and 70 °C.

The operation of batteries at LT can also be achieved by designing additives. Nian and co-workers used the DMSO as an additive to an aqueous electrolyte with a conductivity of 0.11 mS cm^{-1} at −50 °C.[76] MD simulations revealed the mechanism that leads to a lower freezing point following the addition of DMSO. It was found that hydrogen bonds between DMSO and water are more stable than water. As a result, DMSO-water aggregates can prevent the formation of hydrogen-bond-networks typical of freezing.[76]

In SSEs, the diffusion is dominated by hops of ions between neighboring locations, and the diffusivity highly depends on the jump rate and availability of vacant sites.[253] To enable a fast ionic transport, the solid material should have: i) open, and interconnected broad diffusion channels, and ii) a high concentration of carriers. However, introducing more Li ions may decrease the concentration of vacancies, thus eliminating otherwise open diffusion channels. These two strategies should balance in order to improve the ionic conductivity. Fässler and co-workers designed the solid electrolyte Li_9AlP_4 by substituting the Si^{4+} in Li_8SiP_4 with Al^{3+} to increase the concentration of Li ions.[254] This new electrolyte demonstrated a remarkable improvement in ionic conductivity (σ = 3 mS cm^{-1} vs 4.5×10^{-2} mS cm^{-1} for Li_8SiP_4).

Regarding the activation energy, solids are generally characterized by greater E_a compared to liquids.[247] Among SIEs, sulfides have lower activation barriers (E_a = 0.2–0.5 eV) than oxides (E_a = 0.7–1.2 eV). These lower values have been attributed to the high polarizability of the anionic framework of sulfides.[146] Shao-Horn and co-workers investigated the transport mechanism of a series of LISICON type conductors derived from Li_3PO_4 using first-principles calculations and discovered a strong correlation between Li-ion mobility and lattice dynamics.[146] These researchers found that fast Li conductors have the low Li^+ phonon band centered at around ≈40 meV.[146] Zeier et al. followed a similar strategy and substituted the S^{2-} of Na_3PS_4 with the more polarizable Se^{2-} to obtain $Na_3PS_{4-x}Se_x$, successfully observing a lower E_a and a softer lattice.[146,148] An identical approach had also been successfully applied in Li_6PS_5I, where S^{2-} was substituted with Se^{2-}.[144] The produced material Li_6PSe_5I had a lower activation energy (E_a = 0.28 eV vs 0.38 eV for Li_6PS_5I) and a higher conductivity (σ = 0.28 mS cm^{-1} vs 0.0025 mS cm^{-1} for Li_6PS_5I).[144]

5.2. Electrochemical Stability and Interfacial Stability

Besides being a fast ion conductor, an electrolyte needs to be chemically and electrochemically stable with respect to its neighboring electrodes. If this is not the case, the electrolyte will react with the electrodes.[20] Additionally, a more stable electrolyte generally leads to better safety and improved battery performance. The thermodynamic stability of the electrolyte with respect to an electrode can be assessed by computing the difference between the Fermi level of the electrode and the highest occupied molecular orbital (HOMO) or the lowest unoccupied molecular orbital (LUMO) levels of the electrolyte.[20] A too narrow HOMO to LUMO energy difference could lead to electrolyte decomposition at either one of the electrodes depending on their Fermi levels.[255] To prevent the decomposition of LEs, proper additives, e.g., VC,[25] FSE,[26] and FEC,[27,28] have been frequently used. For example, the LUMO energy of FSE (–1.3 eV) was computed to be lower than that of EC (–1.2 eV) and DMC (–1.0), suggesting that the FSE is a better electron acceptor and decomposes before EC and DMC.[26] Zheng et al.[15] performed calculations for LiTFSI-LiBOB dual-salt/CBEs and predicted that LiBOB decomposes at higher voltages than LiTFSI. The more facile reduction of LiBOB relative to that of LiTFSI can effectively protect the LiTFSI from decomposing.

The electrolyte|electrode interface is another critical concern for battery performance. Two types of interfaces are generally preferable: i) a thermodynamically stable interface with no driving force for decomposition reactions; and ii) an interface with a stable SEI with negligible electronic conductivity.[130] Both types of interfaces can prevent the further decomposition of the electrolyte, thus enlarging the electrochemical window. However, a stable SEI can result in lower interfacial resistance, especially if it is too thick or a poor ionic conductor. LiF is widely regarded as a suitable passivation layer as i) LiF, which is an electric insulator, can effectively block electron leakage; and ii) LiF is stable against Li metal and can diffuse Li-ions.[256,257] As a result, forming a LiF-rich SEI layer is an effective strategy often used to stabilize the electrolyte and suppress the growth of Li dendrites. The in situ formation of a LiF-rich layer can be facilitated by the decomposition of the compound containing F, such as LiFSI, FEC. Wang and co-workers have shown that LiFSI has a higher tendency to react with Li metal because of its lower LUMO energy compared to EC and DMC.[257] Zhang et al. reported that FEC is firstly reduced by Li metal in an electrolyte composed of $LiPF_6$ and EC/DEC.[258,259] Both the reduction of LiFSI and FEC led to the formation of a LiF-rich layer, which effectively improved the battery performance.[257–259]

To make LT batteries, it is critical to design electrolyte|electrode interfaces characterized by a low impedance. Introducing Li salts that form ionically conductive SEIs may be conducive to that. Li et al. proposed LiDFBOP as an additive to EC/EMC so that a Li-rich interface could form at both anode and cathode due to LiDFBOP's higher HOMO and lower LUMO energies than those of the solvents.[67] Experimental observations also confirmed the decreased interfacial impedance with the addition of LiDFBOP, whose reduction promoted the in situ formation of the Li-rich SEI films.

Different from the LEs composed of molecules, the electrochemical stability of solid electrolytes can be explored by constructing the grand potential phase diagram (GPPD). The GPPD is constructed by calculating the grand potential ϕ of each phase following

$$\phi = E - \mu_M N_M = E - \left(\mu_M^0 - eV\right)N_M \quad (4)$$

where E is the energy obtained using DFT, μ_M^0 is the chemical potential of alkaline bulk metal M (Li or Na), N_M is the number of M atoms, and V is the applied voltage. The GPPD has been used to i) calculate the electrochemical window of SIEs, i.e., the potential range where the electrolyte is stable upon Li/Na insertion and extraction; and ii) predict the species formed at the electrolyte/electrode interface during charge and discharge at a given V. With the assistance of the GPPD, the electrochemical windows of a variety of solid-state electrolytes have been obtained.[134,152,248] Even though high polarizability of S^{2-} may enhance the ionic conductivity, it also poses limitations for the electrochemical stability. Theoretical calculations demonstrated that sulfides typically have narrow electrochemical windows compared to oxides. It is worth noting that LiF has the highest oxidation potential among binary compounds. This conclusion is consistent with the above argument that LiF can effectively act as a passivation layer to prevent the decomposition of electrolytes and enlarge the electrochemical window. Wang and co-workers formed an in situ LiF-rich SEI layer between Li metal and Li_3PS_4 that was able to effectively suppress the growth of Li dendrites and prevent the reaction between Li_3PS_4 and Li.[260]

5.3. Continuum Models

Continuum level models have been used to obtain the macroscopic electrochemical response of batteries.[261–267] Consequently, they have been extensively used for the design, development, and control of LIBs.[268–275]

The most popular continuum-level model for LIBs is that of Newman and co-workers.[262,267,276–279] This model uses a

pseudo-2D formalism and includes reactions at interfaces and transport in the electrolyte. To account for the dependence of the transport processes and reaction rates on temperature, electrochemical-thermal models derived directly from Newman's model have been developed.[280–285] Notably, it was found that Li diffusion in graphite and concentration polarization issues in the electrolyte limited performance at LT (e.g., −20 °C).[286] Conversely, raising the operating temperature increases the utilization of the electrodes' active materials.[285]

As explained earlier, operating LIBs at HT is a fire hazard. Continuum models have been used to assess the safety of LIBs. For instance, through continuum modeling, the behavior of batteries when they are subjected to extreme conditions can be simulated, including overheating, overcharging, short-circuiting, penetration, and crushing.[287–289] Such adverse circumstances may increase the battery's temperature and eventually lead to a thermal runaway propagating from a cell to the entire pack.[290] Continuum modeling has been instrumental in identifying the factors that promote thermal runaway. For example, Spotnitz et al. found that an increase in the heat released by a single cell and its contact with others in the same pack are two critical factors that can easily trigger thermal runaway.[291] In light of these insights, continuum modeling is now used to design the layout of battery packs and to select the most effective thermal management system.[292,293]

In addition to the thermal issues, continuum modeling is used to investigate the influence of the mechanics of batteries on their electrochemical performance. To study the interfacial instability between electrode particles and solid-state electrolytes, Bucci et al. developed an analytical model that analyzes the delamination of such particles from the surrounding SSE.[294] Moreover, these authors derived a stability condition for fracture propagation within the electrode particles. Thermodynamically consistent electro-chemo-mechanical models that can simulate the dynamic response of an all-solid-state battery have also been developed,[127] showing that due to electric field build-up at the electrode-electrolyte interface, Space charge layers (SCLs) are subjected to considerable stresses. Further, concentrations of reactive species are significantly different from those of the bulk of the material, possibly hampering the kinetics.

The lithium dendrite formation is another safety concern regarding the operation of batteries. Using continuum models, the mechanism of Li deposition and dendrite growth has also been investigated.[295,296] Newman and Monroe proposed one of the first models for a Li-polymer interface and suggested that a separator with a shear modulus twice as large as that of Li can mechanically suppress dendrites.[295,296] However, in their model, the Li was assumed to be defect-free. As such, improving the modulus may not entirely eliminate Li filament formation, as observed in the experiments.[297–299] Phase-field modeling is another frequently used tool to study the dynamic evolution of dendrite growth.[300–303] With the assistance of phase-field simulations, it was proposed that the dendrite growth be effectively suppressed by i) increasing the elastic modulus of the electrolyte,[302] or ii) reducing the exchange current density.[303] Srinivasan also noticed the reduced exchange current density together with the increased elastic modulus of the electrolyte. Later, based on the phase-field simulation results, Viswanathan and co-workers proposed a graded electrolyte with higher local ion concentration as a way to potentially suppress dendrite formation.[300]

In light of the discussion above, and considering the rapid development of novel electrolytes as we outlined in this review, we believe that continuum models can be used to model and develop systems of wide-operable-temperature and safe LIBs.

5.4. Artificial Intelligence Applied to the Discovery of New Electrolytes

AI-assisted models are now starting to be employed for the design of high-performance electrolyte materials in combination with the first-principles calculations. Reed and co-workers first screened candidates from 12 831 Li-containing materials and identified 21 promising solid electrolytes with the potential of delivering high Li ionic conductivity using a logistic regression model.[304] Out of these candidate electrolytes, 10 were further predicted by AIMD simulations to be fast Li conductors ($\sigma \geq 10^{-4}$ S cm^{-1} at RT).[305] In another work done by Mo and co-workers, an unsupervised learning scheme was proposed for discovering new solid lithium fast conductors.[306] Agglomerative hierarchical clustering was used to subdivide the X-ray diffraction patterns of 2986 Li-containing and transition-metal-free compounds into 7 groups. Interestingly, most known lithium conductors with RT σ close to 10^{-3} to 10^{-2} S cm^{-1} were found to be clustered into two groups, i.e., LGPS, $Li_7P_3S_{11}$, LLZO, and Li_3N in group I, and β-Li_3PS_4 and LLTO in group II. AIMD simulations were then carried out for the 82 compounds in groups I and II. Finally, 16 candidates were identified to be Li-conductors with conductivities ranging from 10^{-4} to 10^{-1} S cm^{-1} at RT. Among those, $LiZnPS_4$, which was previously discovered using the bcc-anion-packing rule,[147] was identified. Also, several new compounds, including Li_8N_2Se, Li_6KBiO_6, and $Li_5P_2N_5$ were predicted to be superionic conductors with RT σ above 10^{-2} S cm^{-1}.

In addition to the solid electrolytes, AI models have also been used to design liquids. The ionic transport at the electrolyte/electrode interface is highly correlated to the coordination energy, E_{coord}, of alkali metal ions with the electrolyte solvent. Ishikawa and co-workers predicted the E_{coord} using regression models (e.g., multiple linear regression, least absolute shrinkage and selection operator, and exhaustive search with linear regression) and compared the results obtained by DFT calculations.[307] Okamoto et al. studied the electrochemical activity of additives by predicting their redox potentials using Gaussian kernel ridge and gradient boosting regression.[308] These authors found that even simple descriptors, which were obtained by mapping the molecular structures into a feature space, could predict well the redox potentials, in particular the oxidation potential. Shelton and co-workers investigated the flammability of polymers using the limiting oxygen index as an indicator.[309] In this work, the Gaussian progress regression model was employed, and it was demonstrated this approach could provide an accurate and fast methodology for the development of nonflammable polymers.

The crystal graph convolutional neural network, a model initially developed by the Grossman group to compute the

crystal properties including formation energy, bandgap, and bulk and shear moduli,[310] was shown to predict various molecular features, including HOMO and LUMO energy level, dipole moment, isotropic polarizability, heat capacity, etc.[311] Grossman et al. first trained this AI framework using a dataset consisting of 46 744 materials covering 87 elements, 7 lattice systems, and 216 space groups. These authors found that the model could be used to calculate eight different properties of crystals, including formation energy, bandgap, and elastic constant.[310] Later, the same group applied the same methodology to screen solid electrolytes capable of suppressing Li dendrites.[310] Based on Grossman's work, Chen et al.[311] constructed the MatErials Graph Network (MEGNet). After training on ≈60 000 crystals from the Materials Project database, the MEGNet was shown to outperform other ML models on the QM9 molecule dataset with accuracies for formation energies, bandgaps, and elastic moduli comparable to those of DFT.[312]

6. Conclusion and Perspective

This article reviews the principles underpinning the rational design and fabrication of electrolytes that can deliver high safety while operating over a wide range of temperatures. The performance of relevant and recently developed electrolytes is summarized in **Figure 12**. While there have been significant achievements in this area, new and improved electrolyte materials are needed. **Figure 13** outlines various properties that characterize different types of electrolytes including LEs, GPEs, and SSEs. While LEs have achieved tremendous success with mature industrial production, more efforts are being devoted to GPEs and SSEs, aiming at higher safety. SSEs exhibit the highest safety level. However, poor interfacial contacts with the electrodes and inferior rate capabilities remain mayor bottlenecks of the SSE technology. GPEs can overcome these issues but are also characterized by intrinsic trade-offs. For that, several challenges still need to be addressed. For instance, in-depth investigations of the impact of ionic conductivity, interfacial reactivity, and composition of the electrolyte on the electrochemical performance of devices are needed. DFT and MD have been applied to predict of the electrolyte's conductivities and stability versus voltage and achieved great success in obtaining a number of properties, such as electronic and ionic conductivities, interfacial stabilities, and solvation characteristics. Continuum modeling of electrochemistry is also a powerful tool that has been used to study the electrochemical and thermal response of full batteries and to unravel the mechanism of various phenomena, including dendrite growth. Machine learning has also been used to identify new electrolyte composition. For example, the Oyaizu group[313] fabricated what is currently the largest database of SPEs (up to 10^4 entries), including most of the basic chemical structures, chemical compositions, operating temperatures, and ionic conductivities. Subsequently, the same group successfully employed a transfer-learned graph neural network to predict a new superionic conductor ($\sigma = 10^{-3}$ S cm at RT), which is composed of a glass-type aromatic polymer. It is anticipated that this strategy can help researchers to develop a library of tailored and high-performance electrolytes.

The second challenge comes to the use of the laboratory-based electrolytes in actual devices. This entails meeting both engineering and financial requirements. The particular preparation conditions, low-yields, and expensive precursors used to make lab-scale electrolytes seriously impedes their usage in real applications. To commercialize new high-performance electrolytes, it is critical to use relatively safe and inexpensive reactants and to prepare the materials using cost-effective synthetic processes. While SSEs are attractive for future energy

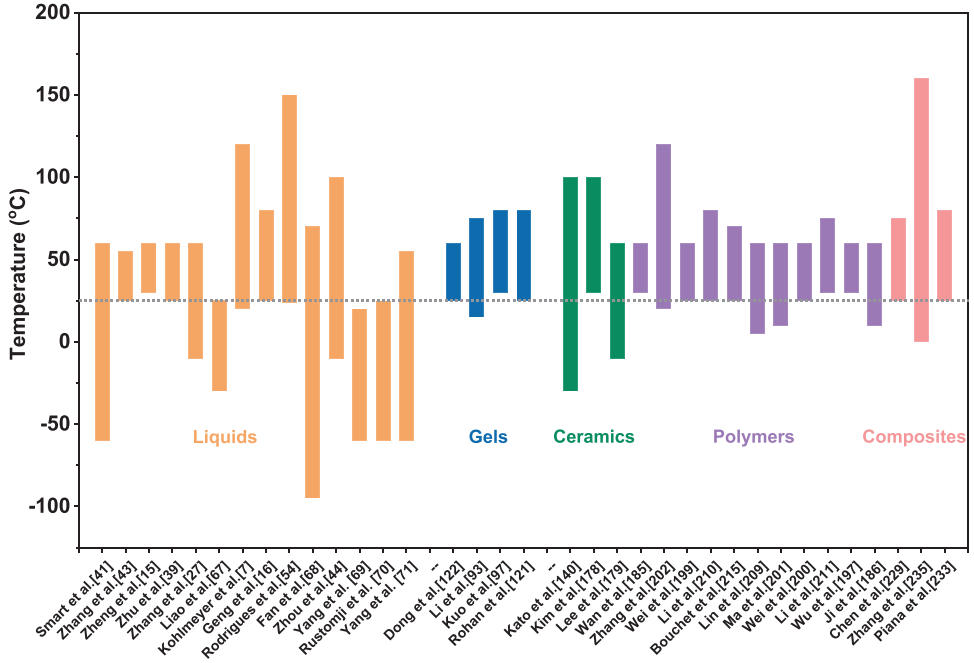

Figure 12. Summary of the operating temperatures of LIBs achieved with different types of electrolyte materials.

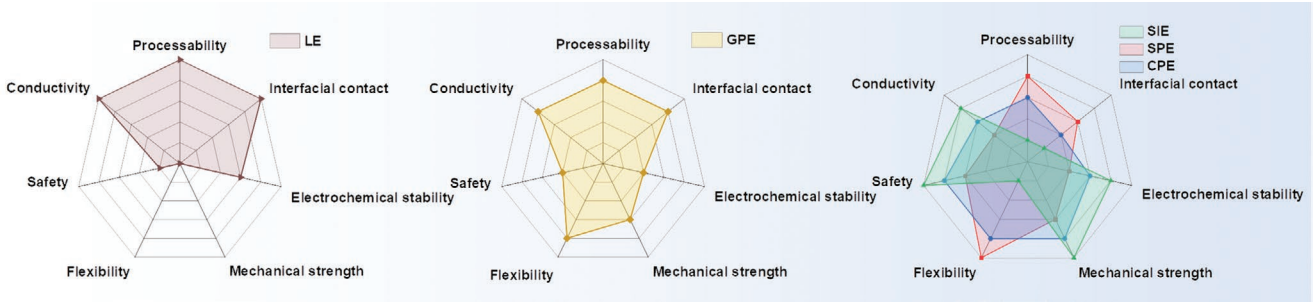

Figure 13. Radar maps of the challenges and strengths different types of electrolytes. Then values (distances from the center) range from 1 to 5, where 5 corresponds to the highest value of a certain property. 0 means certain properties are not applicable to this type of electrolyte.

storage technologies, their large-scale production is still a limiting factor. Various scale-up strategies like mechanochemistry, pressing, sputtering, and tape casting have shown considerable promise as they could lead to making thin and flexible SSE membranes at a scale. It is worth mentioning that a wet coating process has already been employed to fabricate SSBs.[9] Specifically, slurries of electrode material have been fed into a coating machine and spread onto a current collector, which was subsequently coated by an SSE slurry. SSBs can then be made by the bipolar stacking of these components. Further development of cost-effective SSEs manufacturing technologies is expected in the near future.

Electric vehicles require battery systems that can deliver a stable performance while delivering high energy densities even in extreme climates. To meet the requirements, high-voltage cathodes and high-capacity electrodes coupled to electrolytes with a wide electrochemical and temperature window are necessary. Due to their high theoretical capacities, metal-anode-based rechargeable batteries, such as Li-S, Li-air, Na-ion, K-ion, Zn-ion, and Al-ion batteries, have attracted substantial research attention as candidates for next-generation batteries. In this technology, however, the formation of dendrites and brittle SEI layers remains a significant safety concern, especially at extreme temperatures. The development of electrolytes with high ionic conductivity, robust SEI-forming ability, and good electrode wettability at a wide range of temperatures helps to prevent dendrite growth and improve safety.

While several electrolytes with a wide temperature window have been discussed above, most of them contain highly flammable compounds, which may introduce safety issues. To improve their safety, the inclusion of fire-retardants is of great importance. For example, free-standing CPEs composed of PVDF polymer matrices, ceramic fillers, and the flame-retardant TMP have shown to have good nonflammability, high ionic conductivity, flexibility, and excellent thermal stability.[238,314] Recently, the Cui group[315] proposed fireproof, ultralightweight SPEs, composed of a porous PI, a fire-retardant additive (decabromodiphenyl ethane, DBDPE), and PEO/LiTFSI. As a result, LFP/SPE/Li pouch cells showed a high tolerance even under a flame test. However, the working temperature of such electrolytes was limited. Therefore, the combination of nonflammability and a wide temperature window for electrolytes will be a direction and challenge in the future.

Finally, advanced characterization techniques such as cryo-electron microscopy (Cryo-EM),[316] near-edge X-ray absorption fine-structure (NEXAFS) spectroscopy,[317] synchrotron scanning transmission X-ray microscopy (STXM),[318] and neutron diffraction[319] are powerful tools for diagnosing interfacial reactions, ion conduction mechanisms, thermal, physicochemical, and electrochemical properties of battery materials. Recently, in situ scanning electron microscopy (SEM) was employed to monitor the structural evolution of an NMC/SPE/Li cell during cycling at 50 °C.[320] As a result, the progressive decomposition of the SPEs was the principal failure mechanism, which contributed to the outgassing of the cell during cycling. This phenomenon led to a gradual decaying of capacity and efficiency. It is expected that understanding the electrochemical and mechanical phenomena (e.g., dendrite formation, electrolyte decomposition, and SEI generation) observed by such technologies will guide the development of breakthrough electrolyte solutions capable of wide temperature operation.

The emerging electrolytes capable of operating over a wide temperature window and delivering high safety is a very promising direction for the future development of rechargeable energy storage technologies. It is expected that such electrolytes will be used in portable devices, electric vehicles, and perhaps larger-scale energy storage. We anticipate that this review will inspire further work in this area.

Acknowledgements

X.L., G.Z., and J.L. contributed equally to this work. The authors gratefully acknowledge the support of the Hong Kong Innovation and Technology Fund (No. ITS/292/18FP), Research Grants Council of Hong Kong (16207615, 16227016, and 16204517), and the Guangzhou Science and Technology Program (No. 201807010074).

Conflict of Interest

The authors declare no conflict of interest.

Keywords

batteries, electrolytes, safety, temperature window

Received: April 8, 2020
Revised: July 31, 2020
Published online:

[1] P. Albertus, S. Babinec, S. Litzelman, A. Newman, *Nat. Energy* **2018**, *3*, 16.
[2] M. T. F. Rodrigues, G. Babu, H. Gullapalli, K. Kalaga, F. N. Sayed, K. Kato, J. Joyner, P. M. Ajayan, *Nat. Energy* **2017**, *2*, 17108.
[3] J. M. Tarascon, M. Armand, *Nature* **2001**, *414*, 359.
[4] *Nat. Mater.* **2019**, *18*, 1265.
[5] J. Hou, M. Yang, D. Wang, J. Zhang, *Adv. Energy Mater.* **2020**, *10*, 1904152.
[6] G. Crabtree, *Science* **2019**, *366*, 422.
[7] R. R. Kohlmeyer, G. A. Horrocks, A. J. Blake, Z. Yu, B. Maruyama, H. Huang, M. F. Durstock, *Nano Energy* **2019**, *64*, 103927.
[8] B. Zheng, X. Lin, X. Zhang, D. Wu, K. Matyjaszewski, *Adv. Funct. Mater.* **2019**, 1907006.
[9] Y.-S. Hu, *Nat. Energy* **2016**, *1*, 16042.
[10] C. L. Campion, W. Li, B. L. Lucht, *J. Electrochem. Soc.* **2005**, *152*, A2327.
[11] L. Xing, O. Borodin, G. D. Smith, W. Li, *J. Phys. Chem. A* **2011**, *115*, 13896.
[12] Y. Wang, K. Zaghib, A. Guerfi, F. F. C. Bazito, R. M. Torresi, J. R. Dahn, *Electrochim. Acta* **2007**, *52*, 6346.
[13] C. Y. Wang, G. Zhang, S. Ge, T. Xu, Y. Ji, X. G. Yang, Y. Leng, *Nature* **2016**, *529*, 515.
[14] C. R. Sides, C. R. Martin, *Adv. Mater.* **2005**, *17*, 125.
[15] J. M. Zheng, M. H. Engelhard, D. H. Mei, S. H. Jiao, B. J. Polzin, J. G. Zhang, W. Xu, *Nat. Energy* **2017**, *2*, 1.
[16] Z. Geng, J. Lu, Q. Li, J. Qiu, Y. Wang, J. Peng, J. Huang, W. Li, X. Yu, H. Li, *Energy Storage Mater.* **2019**, *23*, 646.
[17] C. Li, S. Liu, C. Shi, G. Liang, Z. Lu, R. Fu, D. Wu, *Nat. Commun.* **2019**, *10*, 1363.
[18] X. Chen, X.-Q. Zhang, H.-R. Li, Q. Zhang, *Batteries Supercaps* **2019**, *2*, 128.
[19] J. B. Goodenough, K. S. Park, *J. Am. Chem. Soc.* **2013**, *135*, 1167.
[20] J. B. Goodenough, Y. Kim, *Chem. Mater.* **2010**, *22*, 587.
[21] B. S. Parimalam, A. D. MacIntosh, R. Kadam, B. L. Lucht, *J. Phys. Chem. C* **2017**, *121*, 22733.
[22] M.-H. Ryou, J.-N. Lee, D. J. Lee, W.-K. Kim, Y. K. Jeong, J. W. Choi, J.-K. Park, Y. M. Lee, *Electrochim. Acta* **2012**, *83*, 259.
[23] M. Herstedt, D. P. Abraham, J. B. Kerr, K. Edström, *Electrochim. Acta* **2004**, *49*, 5097.
[24] J. Kasnatscheew, M. Evertz, B. Streipert, R. Wagner, R. Klopsch, B. Vortmann, H. Hahn, S. Nowak, M. Amereller, A. C. Gentschev, P. Lamp, M. Winter, *Phys. Chem. Chem. Phys.* **2016**, *18*, 3956.
[25] D. Aurbach, K. Gamolsky, B. Markovsky, Y. Gofer, M. Schmidt, U. Heider, *Electrochim. Acta* **2002**, *47*, 1423.
[26] K. Yamagiwa, D. Morita, N. Yabuuchi, T. Tanaka, M. Fukunishi, T. Taki, H. Watanabe, T. Otsuka, T. Yano, J.-Y. Son, Y.-T. Cui, H. Oji, S. Komaba, *Electrochim. Acta* **2015**, *160*, 347.
[27] X. Q. Zhang, X. Chen, X. B. Cheng, B. Q. Li, X. Shen, C. Yan, J. Q. Huang, Q. Zhang, *Angew. Chem., Int. Ed.* **2018**, *57*, 5301.
[28] L. Hu, Z. Zhang, K. Amine, *Electrochem. Commun.* **2013**, *35*, 76.
[29] E. Markevich, G. Salitra, K. Fridman, R. Sharabi, G. Gershinsky, A. Garsuch, G. Semrau, M. A. Schmidt, D. Aurbach, *Langmuir* **2014**, *30*, 7414.
[30] C. Yan, X. B. Cheng, Y. Tian, X. Chen, X. Q. Zhang, W. J. Li, J. Q. Huang, Q. Zhang, *Adv. Mater.* **2018**, *30*, 1707629.
[31] K. Xu, *J. Electrochem. Soc.* **2008**, *155*, A733.
[32] X. Chen, W. Xu, M. H. Engelhard, J. Zheng, Y. Zhang, F. Ding, J. Qian, J.-G. Zhang, *J. Mater. Chem. A* **2014**, *2*, 2346.
[33] S. Shui Zhang, *Electrochem. Commun.* **2006**, *8*, 1423.
[34] Y. Qin, Z. Chen, J. Liu, K. Amine, *Electrochem. Solid-State Lett.* **2010**, *13*, A11.
[35] D. Zhou, W. Li, C. Tan, X. Zuo, Y. Huang, *J. Power Sources* **2008**, *184*, 589.
[36] K. Liu, W. Liu, Y. Qiu, B. Kong, Y. Sun, Z. Chen, D. Zhuo, D. Lin, Y. Cui, *Sci. Adv.* **2017**, *3*, 1601978.
[37] D. Xu, J. Su, J. Jin, C. Sun, Y. Ruan, C. Chen, Z. Wen, *Adv. Energy Mater.* **2019**, *9*, 938.
[38] H. Yang, C. Guo, J. Chen, A. Naveed, J. Yang, Y. Nuli, J. Wang, *Angew. Chem., Int. Ed.* **2019**, *58*, 791.
[39] Y. Zhu, X. Luo, H. Zhi, Y. Liao, L. Xing, M. Xu, X. Liu, K. Xu, W. Li, *J. Mater. Chem. A* **2018**, *6*, 10990.
[40] J. Kalhoff, G. G. Eshetu, D. Bresser, S. Passerini, *ChemSusChem* **2015**, *8*, 2154.
[41] M. C. Smart, B. V. Ratnakumar, K. B. Chin, L. D. Whitcanack, *J. Electrochem. Soc.* **2010**, *157*, A1361.
[42] M. C. Smart, B. L. Lucht, S. Dalavi, F. C. Krause, B. V. Ratnakumar, *J. Electrochem. Soc.* **2012**, *159*, A739.
[43] Z. C. Zhang, L. B. Hu, H. M. Wu, W. Weng, M. Koh, P. C. Redfern, L. A. Curtiss, K. Amine, *Energy Environ. Sci.* **2013**, *6*, 1806.
[44] Q. Zhou, S. Dong, Z. Lv, G. Xu, L. Huang, Q. Wang, Z. Cui, G. Cui, *Adv. Energy Mater.* **2020**, *10*, 1903441.
[45] M. Galiński, A. Lewandowski, I. Stępniak, *Electrochim. Acta* **2006**, *51*, 5567.
[46] Y. Qiao, Y. He, K. Jiang, Y. Liu, X. Li, M. Jia, S. Guo, H. Zhou, *Adv. Energy Mater.* **2018**, *8*, 1802322.
[47] A. Balducci, R. Dugas, P. L. Taberna, P. Simon, D. Plée, M. Mastragostino, S. Passerini, *J. Power Sources* **2007**, *165*, 922.
[48] D. Monti, E. Jónsson, M. R. Palacín, P. Johansson, *J. Power Sources* **2014**, *245*, 630.
[49] G. B. Appetecchi, M. Montanino, M. Carewska, M. Moreno, F. Alessandrini, S. Passerini, *Electrochim. Acta* **2011**, *56*, 1300.
[50] G.-T. Kim, G. B. Appetecchi, F. Alessandrini, S. Passerini, *J. Power Sources* **2007**, *171*, 861.
[51] M. K. P. Johansson, *Batteries* **2018**, *4*, 10.
[52] N. Plylahan, M. Kerner, D.-H. Lim, A. Matic, P. Johansson, *Electrochim. Acta* **2016**, *216*, 24.
[53] G. A. Elia, U. Ulissi, S. Jeong, S. Passerini, J. Hassoun, *Energy Environ. Sci.* **2016**, *9*, 3210.
[54] M.-T. F. Rodrigues, K. Kalaga, H. Gullapalli, G. Babu, A. L. M. Reddy, P. M. Ajayan, *Adv. Energy Mater.* **2016**, *6*, 1600218.
[55] P. G. Bruce, S. A. Freunberger, L. J. Hardwick, J. M. Tarascon, *Nat. Mater.* **2012**, *11*, 19.
[56] X. Lin, G. Xie, S. Liu, M. R. Martinez, Z. Wang, H. Lou, R. Fu, D. Wu, K. Matyjaszewski, *ACS Appl. Mater. Interfaces* **2019**, *11*, 18763.
[57] X. Lin, Y. Liang, Z. Lu, H. Lou, X. Zhang, S. Liu, B. Zheng, R. Liu, R. Fu, D. Wu, *ACS Sustainable Chem. Eng.* **2017**, *5*, 8535.
[58] S. Liu, J. Li, X. Yan, Q. Su, Y. Lu, J. Qiu, Z. Wang, X. Lin, J. Huang, R. Liu, B. Zheng, L. Chen, R. Fu, D. Wu, *Adv. Mater.* **2018**, *30*, 1706895.
[59] F. Xu, Z. Tang, S. Huang, L. Chen, Y. Liang, W. Mai, H. Zhong, R. Fu, D. Wu, *Nat. Commun.* **2015**, *6*, 7221.
[60] J. Wu, J. Liu, Z. Lu, K. Lin, Y.-Q. Lyu, B. Li, F. Ciucci, J.-K. Kim, *Energy Storage Mater.* **2019**, *23*, 8.
[61] M. C. Smart, *J. Electrochem. Soc.* **1999**, *146*, 486.
[62] X. Dong, Y. Lin, P. Li, Y. Ma, J. Huang, D. Bin, Y. Wang, Y. Qi, Y. Xia, *Angew. Chem., Int. Ed.* **2019**, *58*, 5623.
[63] L. Liao, X. Cheng, Y. Ma, P. Zuo, W. Fang, G. Yin, Y. Gao, *Electrochim. Acta* **2013**, *87*, 466.
[64] L. Liao, T. Fang, X. Zhou, Y. Gao, X. Cheng, L. Zhang, G. Yin, *Solid State Ionics* **2014**, *254*, 27.
[65] S. S. Zhang, K. Xu, T. R. Jow, *Electrochem. Commun.* **2002**, *4*, 928.
[66] M. C. Smart, B. V. Ratnakumar, S. Surampudi, *J. Electrochem. Soc.* **2002**, *149*, A361.
[67] B. Liao, H. Li, M. Xu, L. Xing, Y. Liao, X. Ren, W. Fan, L. Yu, K. Xu, W. Li, *Adv. Energy Mater.* **2018**, *8*, 1800802.
[68] X. Fan, X. Ji, L. Chen, J. Chen, T. Deng, F. Han, J. Yue, N. Piao, R. Wang, X. Zhou, X. Xiao, L. Chen, C. Wang, *Nat. Energy* **2019**, *4*, 882.
[69] Y. Yang, D. M. Davies, Y. Yin, O. Borodin, J. Z. Lee, C. Fang, M. Olguin, Y. Zhang, E. S. Sablina, X. Wang, C. S. Rustomji, Y. S. Meng, *Joule* **2019**, *3*, 1986.

[70] C. S. Rustomji, Y. Yang, T. K. Kim, J. Mac, Y. J. Kim, E. Caldwell, H. Chung, Y. S. Meng, *Science* **2017**, *356*, eaal4263.
[71] Y. Yang, Y. Yin, D. M. Davies, M. Zhang, M. Mayer, Y. Zhang, E. S. Sablina, S. Wang, J. Z. Lee, O. Borodin, C. S. Rustomji, Y. S. Meng, *Energy Environ. Sci.* **2020**, *13*, 2209.
[72] G. G. Eshetu, G. A. Elia, M. Armand, M. Forsyth, S. Komaba, T. Rojo, S. Passerini, *Adv. Energy Mater.* **2020**, *10*, 2000093.
[73] C. Yang, S. Xin, L. Mai, Y. You, *Adv. Energy Mater.* **2020**, 2000974.
[74] Y. You, H.-R. Yao, S. Xin, Y.-X. Yin, T.-T. Zuo, C.-P. Yang, Y.-G. Guo, Y. Cui, L.-J. Wan, J. B. Goodenough, *Adv. Mater.* **2016**, *28*, 7243.
[75] J.-Z. Guo, P.-F. Wang, X.-L. Wu, X.-H. Zhang, Q. Yan, H. Chen, J.-P. Zhang, Y.-G. Guo, *Adv. Mater.* **2017**, *29*, 1701968.
[76] Y.-Y. Wang, B.-H. Hou, J.-Z. Guo, Q.-L. Ning, W.-L. Pang, J. Wang, C.-L. Lü, X.-L. Wu, *Adv. Energy Mater.* **2018**, *8*, 1703252.
[77] B.-H. Hou, Y.-Y. Wang, D.-S. Liu, Z.-Y. Gu, X. Feng, H. Fan, T. Zhang, C. Lü, X.-L. Wu, *Adv. Funct. Mater.* **2018**, *28*, 1805444.
[78] Y. P. Wu, X. B. Dai, J. Q. Ma, Y. J. Chen, *Lithium Ion Batteries: Practice and Applications*, Chemical Industry, Beijing **2004**.
[79] Q. Nian, J. Wang, S. Liu, T. Sun, S. Zheng, Y. Zhang, Z. Tao, J. Chen, *Angew. Chem., Int. Ed.* **2019**, *58*, 16994.
[80] N. Wang, X. Dong, B. Wang, Z. Guo, Z. Wang, R. Wang, X. Qiu, Y. Wang, *Angew. Chem., Int. Ed.* **2020**, *59*, 14577.
[81] X. Cheng, J. Pan, Y. Zhao, M. Liao, H. Peng, *Adv. Energy Mater.* **2018**, *8*, 1702184.
[82] K. S. Ngai, S. Ramesh, K. Ramesh, J. C. Juan, *Ionics* **2016**, *22*, 1259.
[83] H. y. Sung, Y. y. Wang, C. c. Wan, *J. Electrochem. Soc.* **1998**, *145*, 1207.
[84] N. S. Mohamed, A. K. Arof, *J. Power Sources* **2004**, *132*, 229.
[85] H.-S. Kim, S.-I. Moon, *J. Power Sources* **2005**, *146*, 584.
[86] J. J. Xu, H. Ye, *Electrochem. Commun.* **2005**, *7*, 829.
[87] C.-Y. Hsu, R.-J. Liu, C.-H. Hsu, P.-L. Kuo, *RSC Adv.* **2016**, *6*, 18082.
[88] Y. Kato, K. Hasumi, S. Yokoyama, T. Yabe, H. Ikuta, Y. Uchimoto, M. Wakihara, *Solid State Ionics* **2002**, *150*, 355.
[89] S. Zhang, J. Cao, Y. Shang, L. Wang, X. He, J. Li, P. Zhao, Y. Wang, *J. Mater. Chem. A* **2015**, *3*, 17697.
[90] W. Chen, Y. Liu, Y. Ma, W. Yang, *J. Power Sources* **2015**, *273*, 1127.
[91] B. Kurc, *Electrochim. Acta* **2014**, *125*, 415.
[92] H.-S. Jeong, D.-W. Kim, Y. U. Jeong, S.-Y. Lee, *J. Power Sources* **2010**, *195*, 6116.
[93] Z. Li, G. Su, X. Wang, D. Gao, *Solid State Ionics* **2005**, *176*, 1903.
[94] D. Song, C. Xu, Y. Chen, J. He, Y. Zhao, P. Li, W. Lin, F. Fu, *Solid State Ionics* **2015**, *282*, 31.
[95] H. Nakajima, H. Ohno, *Polymer* **2005**, *46*, 11499.
[96] D. Zhou, R. Liu, J. Zhang, X. Qi, Y.-B. He, B. Li, Q.-H. Yang, Y.-S. Hu, F. Kang, *Nano Energy* **2017**, *33*, 45.
[97] P.-L. Kuo, C.-H. Tsao, C.-H. Hsu, S.-T. Chen, H.-M. Hsu, *J. Membr. Sci.* **2016**, *499*, 462.
[98] G. T. Kim, S. S. Jeong, M. Z. Xue, A. Balducci, M. Winter, S. Passerini, F. Alessandrini, G. B. Appetecchi, *J. Power Sources* **2012**, *199*, 239.
[99] G. B. Appetecchi, M. Montanino, S. Passerini, in *Ionic Liquids: Science and Applications*, Vol. *1117*, American Chemical Society, Washington, DC **2012**, p. 67.
[100] N. Shirshova, A. Bismarck, S. Carreyette, Q. P. V. Fontana, E. S. Greenhalgh, P. Jacobsson, P. Johansson, M. J. Marczewski, G. Kalinka, A. R. J. Kucernak, J. Scheers, M. S. P. Shaffer, J. H. G. Steinke, M. Wienrich, *J. Mater. Chem. A* **2013**, *1*, 15300.
[101] A. Boschin, P. Johansson, *Electrochim. Acta* **2016**, *211*, 1006.
[102] D. Zhou, Y. B. He, R. L. Liu, M. Liu, H. D. Du, B. H. Li, Q. Cai, Q. H. Yang, F. Y. Kang, *Adv. Energy Mater.* **2015**, *5*, 1500353.
[103] J. Chen, Z. Yang, G. Liu, C. Li, J. Yi, M. Fan, H. Tan, Z. Lu, C. Yang, *Energy Storage Mater.* **2020**, *25*, 305.
[104] X. Xu, K. Lin, D. Zhou, Q. Liu, X. Qin, S. Wang, S. He, F. Kang, B. Li, G. Wang, *Chem* **2020**, *6*, 902.
[105] M.-K. Song, J.-Y. Cho, B. W. Cho, H.-W. Rhee, *J. Power Sources* **2002**, *110*, 209.
[106] B. Rupp, M. Schmuck, A. Balducci, M. Winter, W. Kern, *Eur. Polym. J.* **2008**, *44*, 2986.
[107] J. R. Nair, C. Gerbaldi, G. Meligrana, R. Bongiovanni, S. Bodoardo, N. Penazzi, P. Reale, V. Gentili, *J. Power Sources* **2008**, *178*, 751.
[108] C. Gerbaldi, J. R. Nair, S. Ahmad, G. Meligrana, R. Bongiovanni, S. Bodoardo, N. Penazzi, *J. Power Sources* **2010**, *195*, 1706.
[109] C. Gerbaldi, J. R. Nair, G. Meligrana, R. Bongiovanni, S. Bodoardo, N. Penazzi, *Electrochim. Acta* **2010**, *55*, 1460.
[110] J.-H. Baik, S. Kim, D. G. Hong, J.-C. Lee, *ACS Appl. Mater. Interfaces* **2019**, *11*, 29718.
[111] L. Porcarelli, C. Gerbaldi, F. Bella, J. R. Nair, *Sci. Rep.* **2016**, *6*, 19892.
[112] R. Hagiwara, Y. Ito, *J. Fluorine Chem.* **2000**, *105*, 221.
[113] Y.-S. Ye, J. Rick, B.-J. Hwang, *J. Mater. Chem. A* **2013**, *1*, 2719.
[114] D. R. MacFarlane, N. Tachikawa, M. Forsyth, J. M. Pringle, P. C. Howlett, G. D. Elliott, J. H. Davis, M. Watanabe, P. Simon, C. A. Angell, *Energy Environ. Sci.* **2014**, *7*, 232.
[115] Y. Lu, S. S. Moganty, J. L. Schaefer, L. A. Archer, *J. Mater. Chem.* **2012**, *22*, 4066.
[116] K. Yin, Z. Zhang, L. Yang, S.-I. Hirano, *J. Power Sources* **2014**, *258*, 150.
[117] Y. Lu, K. Korf, Y. Kambe, Z. Tu, L. A. Archer, *Angew. Chem., Int. Ed.* **2014**, *53*, 488.
[118] A.-L. Pont, R. Marcilla, I. De Meatza, H. Grande, D. Mecerreyes, *J. Power Sources* **2009**, *188*, 558.
[119] L. T. Costa, B. Sun, F. Jeschull, D. Brandell, *J. Chem. Phys.* **2015**, *143*, 024904.
[120] K. Angenendt, P. Johansson, *J. Phys. Chem. B* **2011**, *115*, 7808.
[121] R. Rohan, K. Pareek, Z. Chen, W. Cai, Y. Zhang, G. Xu, Z. Gao, H. Cheng, *J. Mater. Chem. A* **2015**, *3*, 20267.
[122] T. Dong, J. Zhang, G. Xu, J. Chai, H. Du, L. Wang, H. Wen, X. Zang, A. Du, Q. Jia, X. Zhou, G. Cui, *Energy Environ. Sci.* **2018**, *11*, 1197.
[123] M. S. Zhu, X. J. Wang, H. M. Tang, J. W. Wang, Q. Hao, L. X. Liu, Y. Li, K. Zhang, O. G. Schmidt, *Adv. Funct. Mater.* **2020**, *30*, 1907218.
[124] F. Mo, G. Liang, Q. Meng, Z. Liu, H. Li, J. Fan, C. Zhi, *Energy Environ. Sci.* **2019**, *12*, 706.
[125] Z. Gao, H. Sun, L. Fu, F. Ye, Y. Zhang, W. Luo, Y. Huang, *Adv. Mater.* **2018**, *30*, 1705702.
[126] H. Lee, P. Oh, J. Kim, H. Cha, S. Chae, S. Lee, J. Cho, *Adv. Mater.* **2019**, *31*, 1900376.
[127] T. H. Wan, F. Ciucci, *Electrochim. Acta* **2020**, *331*, 135355.
[128] Y.-Q. Lyu, J. Yu, J. Wu, M. B. Effat, F. Ciucci, *J. Power Sources* **2019**, *416*, 21.
[129] D. H. S. Tan, A. Banerjee, Z. Chen, Y. S. Meng, *Nat. Nanotechnol.* **2020**, *15*, 170.
[130] Y. Xiao, Y. Wang, S.-H. Bo, J. C. Kim, L. J. Miara, G. Ceder, *Nat. Rev. Mater.* **2020**, *5*, 105.
[131] N. Ohta, K. Takada, L. Zhang, R. Ma, M. Osada, T. Sasaki, *Adv. Mater.* **2006**, *18*, 2226.
[132] N. Ohta, K. Takada, I. Sakaguchi, L. Zhang, R. Ma, K. Fukuda, M. Osada, T. Sasaki, *Electrochem. Commun.* **2007**, *9*, 1486.
[133] A. M. Nolan, Y. Zhu, X. He, Q. Bai, Y. Mo, *Joule* **2018**, *2*, 2016.
[134] Y. Zhu, X. He, Y. Mo, *J. Mater. Chem. A* **2016**, *4*, 3253.
[135] M. Saccoccio, J. Yu, Z. Lu, S. C. T. Kwok, J. Wang, K. K. Yeung, M. M. F. Yuen, F. Ciucci, *J. Power Sources* **2017**, *365*, 43.
[136] L. Yue, J. Ma, J. Zhang, J. Zhao, S. Dong, Z. Liu, G. Cui, L. Chen, *Energy Storage Mater.* **2016**, *5*, 139.
[137] A. Manthiram, X. Yu, S. Wang, *Nat. Rev. Mater.* **2017**, *2*, 16103.
[138] L. Fan, S. Wei, S. Li, Q. Li, Y. Lu, *Adv. Energy Mater.* **2018**, *8*, 1702657.
[139] N. Kamaya, K. Homma, Y. Yamakawa, M. Hirayama, R. Kanno, M. Yonemura, T. Kamiyama, Y. Kato, S. Hama, K. Kawamoto, *Nat. Mater.* **2011**, *10*, 682.

[140] Y. Kato, S. Hori, T. Saito, K. Suzuki, M. Hirayama, A. Mitsui, M. Yonemura, H. Iba, R. Kanno, *Nat. Energy* **2016**, *1*, 16030.
[141] Y. Seino, T. Ota, K. Takada, A. Hayashi, M. Tatsumisago, *Energy Environ. Sci.* **2014**, *7*, 627.
[142] M. A. Kraft, S. Ohno, T. Zinkevich, R. Koerver, S. P. Culver, T. Fuchs, A. Senyshyn, S. Indris, B. J. Morgan, W. G. Zeier, *J. Am. Chem. Soc.* **2018**, *140*, 16330.
[143] L. Zhou, A. Assoud, Q. Zhang, X. Wu, L. F. Nazar, *J. Am. Chem. Soc.* **2019**, *141*, 19002.
[144] R. Schlem, M. Ghidiu, S. P. Culver, A.-L. Hansen, W. G. Zeier, *ACS Appl. Energy Mater.* **2020**, *3*, 9.
[145] J. C. Bachman, S. Muy, A. Grimaud, H. H. Chang, N. Pour, S. F. Lux, O. Paschos, F. Maglia, S. Lupart, P. Lamp, L. Giordano, Y. Shao-Horn, *Chem. Rev.* **2016**, *116*, 140.
[146] S. Muy, J. C. Bachman, L. Giordano, H.-H. Chang, D. L. Abernathy, D. Bansal, O. Delaire, S. Hori, R. Kanno, F. Maglia, S. Lupart, P. Lamp, Y. Shao-Horn, *Energy Environ. Sci.* **2018**, *11*, 850.
[147] Y. Wang, W. D. Richards, S. P. Ong, L. J. Miara, J. C. Kim, Y. Mo, G. Ceder, *Nat. Mater.* **2015**, *14*, 1026.
[148] T. Krauskopf, S. Muy, S. P. Culver, S. Ohno, O. Delaire, Y. Shao-Horn, W. G. Zeier, *J. Am. Chem. Soc.* **2018**, *140*, 14464.
[149] M. A. Kraft, S. P. Culver, M. Calderon, F. Bocher, T. Krauskopf, A. Senyshyn, C. Dietrich, A. Zevalkink, J. Janek, W. G. Zeier, *J. Am. Chem. Soc.* **2017**, *139*, 10909.
[150] F. Han, Y. Zhu, X. He, Y. Mo, C. Wang, *Adv. Energy Mater.* **2016**, *6*, 1501590.
[151] F. Han, T. Gao, Y. Zhu, K. J. Gaskell, C. Wang, *Adv. Mater.* **2015**, *27*, 3473.
[152] Y. Zhu, X. He, Y. Mo, *ACS Appl. Mater. Interfaces* **2015**, *7*, 23685.
[153] T. Thompson, J. Wolfenstine, J. L. Allen, M. Johannes, A. Huq, I. N. David, J. Sakamoto, *J. Mater. Chem. A* **2014**, *2*, 13431.
[154] A. Sharafi, H. M. Meyer, J. Nanda, J. Wolfenstine, J. Sakamoto, *J. Power Sources* **2016**, *302*, 135.
[155] J. Awaka, N. Kijima, H. Hayakawa, J. Akimoto, *J. Solid State Chem.* **2009**, *182*, 2046.
[156] C. Ma, Y. Cheng, K. Yin, J. Luo, A. Sharafi, J. Sakamoto, J. Li, K. L. More, N. J. Dudney, M. Chi, *Nano Lett.* **2016**, *16*, 7030.
[157] R. H. Brugge, J. A. Kilner, A. Aguadero, *Solid State Ionics* **2019**, *337*, 154.
[158] R. Wagner, G. J. Redhammer, D. Rettenwander, A. Senyshyn, W. Schmidt, M. Wilkening, G. Amthauer, *Chem. Mater.* **2016**, *28*, 1861.
[159] J. L. Allen, J. Wolfenstine, E. Rangasamy, J. Sakamoto, *J. Power Sources* **2012**, *206*, 315.
[160] A. Logéat, T. Köhler, U. Eisele, B. Stiaszny, A. Harzer, M. Tovar, A. Senyshyn, H. Ehrenberg, B. Kozinsky, *Solid State Ionics* **2012**, *206*, 33.
[161] Y. Li, C.-A. Wang, H. Xie, J. Cheng, J. B. Goodenough, *Electrochem. Commun.* **2011**, *13*, 1289.
[162] Z. Zhang, Q. Zhang, J. Shi, Y. S. Chu, X. Yu, K. Xu, M. Ge, H. Yan, W. Li, L. Gu, Y.-S. Hu, H. Li, X.-Q. Yang, L. Chen, X. Huang, *Adv. Energy Mater.* **2017**, *7*.
[163] S. Stramare, V. Thangadurai, W. Weppner, *Chem. Mater.* **2003**, *15*, 3974.
[164] B. Huang, B. Xu, Y. Li, W. Zhou, Y. You, S. Zhong, C. A. Wang, J. B. Goodenough, *ACS Appl. Mater. Interfaces* **2016**, *8*, 14552.
[165] Y. Li, H. Xu, P. H. Chien, N. Wu, S. Xin, L. Xue, K. Park, Y. Y. Hu, J. B. Goodenough, *Angew. Chem., Int. Ed.* **2018**, *57*, 8587.
[166] Y. Zhao, L. L. Daemen, *J. Am. Chem. Soc.* **2012**, *134*, 15042.
[167] Z. D. Hood, H. Wang, A. Samuthira Pandian, J. K. Keum, C. Liang, *J. Am. Chem. Soc.* **2016**, *138*, 1768.
[168] Y. Li, W. Zhou, S. Xin, S. Li, J. Zhu, X. Lu, Z. Cui, Q. Jia, J. Zhou, Y. Zhao, J. B. Goodenough, *Angew. Chem., Int. Ed.* **2016**, *55*, 9965.
[169] B. Kumar, D. Thomas, J. Kumar, *J. Electrochem. Soc.* **2009**, *156*, A506.
[170] X. Han, Y. Gong, K. K. Fu, X. He, G. T. Hitz, J. Dai, A. Pearse, B. Liu, H. Wang, G. Rubloff, Y. Mo, V. Thangadurai, E. D. Wachsman, L. Hu, *Nat. Mater.* **2017**, *16*, 572.
[171] W. Luo, Y. Gong, Y. Zhu, Y. Li, Y. Yao, Y. Zhang, K. K. Fu, G. Pastel, C. F. Lin, Y. Mo, E. D. Wachsman, L. Hu, *Adv. Mater.* **2017**, *29*, 1606042.
[172] C. Wang, Y. Gong, B. Liu, K. Fu, Y. Yao, E. Hitz, Y. Li, J. Dai, S. Xu, W. Luo, E. D. Wachsman, L. Hu, *Nano Lett.* **2017**, *17*, 565.
[173] S. Ohta, S. Komagata, J. Seki, T. Saeki, S. Morishita, T. Asaoka, *J. Power Sources* **2013**, *238*, 53.
[174] K. Park, B.-C. Yu, J.-W. Jung, Y. Li, W. Zhou, H. Gao, S. Son, J. B. Goodenough, *Chem. Mater.* **2016**, *28*, 8051.
[175] S. Ohta, J. Seki, Y. Yagi, Y. Kihira, T. Tani, T. Asaoka, *J. Power Sources* **2014**, *265*, 40.
[176] J. van den Broek, S. Afyon, J. L. M. Rupp, *Adv. Energy Mater.* **2016**, *6*, 1600736.
[177] K. Fu, Y. Gong, G. T. Hitz, D. W. McOwen, Y. Li, S. Xu, Y. Wen, L. Zhang, C. Wang, G. Pastel, J. Dai, B. Liu, H. Xie, Y. Yao, E. D. Wachsman, L. Hu, *Energy Environ. Sci.* **2017**, *10*, 1568.
[178] D. H. Kim, D. Y. Oh, K. H. Park, Y. E. Choi, Y. J. Nam, H. A. Lee, S. M. Lee, Y. S. Jung, *Nano Lett.* **2017**, *17*, 3013.
[179] Y.-G. Lee, S. Fujiki, C. Jung, N. Suzuki, N. Yashiro, R. Omoda, D.-S. Ko, T. Shiratsuchi, T. Sugimoto, S. Ryu, J. H. Ku, T. Watanabe, Y. Park, Y. Aihara, D. Im, I. T. Han, *Nat. Energy* **2020**, *5*, 299.
[180] S. Li, W. Zhang, J. Zheng, M. Lv, H. Song, L. Du, *Adv. Energy Mater.* **2020**, 2000779.
[181] Q. Han, X. Li, X. Shi, H. Zhang, D. Song, F. Ding, L. Zhang, *J. Mater. Chem. A* **2019**, *7*, 3895.
[182] C. Wang, W. Ping, Q. Bai, H. Cui, R. Hensleigh, R. Wang, A. H. Brozena, Z. Xu, J. Dai, Y. Pei, C. Zheng, G. Pastel, J. Gao, X. Wang, H. Wang, J. C. Zhao, B. Yang, X. R. Zheng, J. Luo, Y. Mo, B. Dunn, L. Hu, *Science* **2020**, *368*, 521.
[183] M. J. Wang, R. Choudhury, J. Sakamoto, *Joule* **2019**, *3*, 2165.
[184] D. M. Pesko, M. A. Webb, Y. Jung, Q. Zheng, T. F. Miller, G. W. Coates, N. P. Balsara, *Macromolecules* **2016**, *49*, 5244.
[185] J. Wan, J. Xie, X. Kong, Z. Liu, K. Liu, F. Shi, A. Pei, H. Chen, W. Chen, J. Chen, X. Zhang, L. Zong, J. Wang, L. Q. Chen, J. Qin, Y. Cui, *Nat. Nanotechnol.* **2019**, *14*, 705.
[186] X. Ji, H. Zeng, X. Gong, F. Tsai, T. Jiang, R. K. Y. Li, H. Shi, S. Luan, D. Shi, *J. Mater. Chem. A* **2017**, *5*, 24444.
[187] C. Wang, T. Wang, L. Wang, Z. Hu, Z. Cui, J. Li, S. Dong, X. Zhou, G. Cui, *Adv. Sci.* **2019**, *6*, 1901036.
[188] J. Chai, Z. Liu, J. Ma, J. Wang, X. Liu, H. Liu, J. Zhang, G. Cui, L. Chen, *Adv. Sci.* **2017**, *4*, 1600377.
[189] Y. Tominaga, K. Yamazaki, *Chem. Commun.* **2014**, *50*, 4448.
[190] B. Sun, J. Mindemark, K. Edström, D. Brandell, *Solid State Ionics* **2014**, *262*, 738.
[191] B. Sun, J. Mindemark, K. Edström, D. Brandell, *Electrochem. Commun.* **2015**, *52*, 71.
[192] D. H. Wong, J. L. Thelen, Y. Fu, D. Devaux, A. A. Pandya, V. S. Battaglia, N. P. Balsara, J. M. DeSimone, *Proc. Natl. Acad. Sci. USA* **2014**, *111*, 3327.
[193] X. Zhang, S. Wang, C. Xue, C. Xin, Y. Lin, Y. Shen, L. Li, C. W. Nan, *Adv. Mater.* **2019**, *31*, 1806082.
[194] W. H. Meyer, *Adv. Mater.* **1998**, *10*, 439.
[195] A. Manuel Stephan, K. S. Nahm, *Polymer* **2006**, *47*, 5952.
[196] J. M. Whiteley, P. Taynton, W. Zhang, S. H. Lee, *Adv. Mater.* **2015**, *27*, 6922.
[197] J. Wu, Z. Rao, Z. Cheng, L. Yuan, Z. Li, Y. Huang, *Adv. Energy Mater.* **2019**, *9*, 1902767.
[198] X. Chen, W. He, L.-X. Ding, S. Wang, H. Wang, *Energy Environ. Sci.* **2019**, *12*, 938.
[199] Z. Y. Wei, S. J. Chen, J. Y. Wang, Z. H. Wang, Z. H. Zhang, X. Y. Yao, Y. H. Deng, X. X. Xu, *J. Mater. Chem. A* **2018**, *6*, 13438.
[200] Z. Y. Wei, Z. H. Zhang, S. J. Chen, Z. H. Wang, X. Y. Yao, Y. H. Deng, X. X. Xu, *Energy Storage Mater.* **2019**, *22*, 337.

[201] C. Ma, Y. Feng, F. Xing, L. Zhou, Y. Yang, Q. Xia, L. Zhou, L. Zhang, L. Chen, D. G. Ivey, D. R. Sadoway, W. Wei, *J. Mater. Chem. A* **2019**, *7*, 19970.
[202] J. Zhang, J. Zhao, L. Yue, Q. Wang, J. Chai, Z. Liu, X. Zhou, H. Li, Y. Guo, G. Cui, L. Chen, *Adv. Energy Mater.* **2015**, *5*, 1501082.
[203] A. M. Christie, S. J. Lilley, E. Staunton, Y. G. Andreev, P. G. Bruce, *Nature* **2005**, *433*, 50.
[204] M. Echeverri, C. Hamad, T. Kyu, *Solid State Ionics* **2014**, *254*, 92.
[205] D. Lin, P. Y. Yuen, Y. Liu, W. Liu, N. Liu, R. H. Dauskardt, Y. Cui, *Adv. Mater.* **2018**, *30*, 1802661.
[206] Z. Lu, J. Yu, J. Wu, M. B. Effat, S. C. T. Kwok, Y. Lyu, M. M. F. Yuen, F. Ciucci, *Energy Storage Mater.* **2019**, *18*, 311.
[207] M. B. Effat, Z. Lu, A. Belotti, J. Yu, Y.-Q. Lyu, F. Ciucci, *J. Power Sources* **2019**, *436*, 226802.
[208] L. Porcarelli, A. S. Shaplov, F. Bella, J. R. Nair, D. Mecerreyes, C. Gerbaldi, *ACS Energy Lett.* **2016**, *1*, 678.
[209] Z. Lin, X. Guo, H. Yu, *Nano Energy* **2017**, *41*, 646.
[210] X. Li, Z. Zhang, S. Li, K. Yang, L. Yang, *J. Mater. Chem. A* **2017**, *5*, 21362.
[211] S. Li, Y.-M. Chen, W. Liang, Y. Shao, K. Liu, Z. Nikolov, Y. Zhu, *Joule* **2018**, *2*, 1838.
[212] G. Xie, X. Lin, M. R. Martinez, Z. Wang, H. Lou, R. Fu, D. Wu, K. Matyjaszewski, *Chem. Mater.* **2018**, *30*, 8624.
[213] J. L. Wu, F. Xu, S. M. Li, P. W. Ma, X. C. Zhang, Q. H. Liu, R. W. Fu, D. C. Wu, *Adv. Mater.* **2019**, *31*, 1802922.
[214] D. Zhou, A. Tkacheva, X. Tang, B. Sun, D. Shanmukaraj, P. Li, F. Zhang, M. Armand, G. Wang, *Angew. Chem., Int. Ed.* **2019**, *58*, 6001.
[215] R. Bouchet, S. Maria, R. Meziane, A. Aboulaich, L. Lienafa, J. P. Bonnet, T. N. Phan, D. Bertin, D. Gigmes, D. Devaux, R. Denoyel, M. Armand, *Nat. Mater.* **2013**, *12*, 452.
[216] K. Deng, J. Qin, S. Wang, S. Ren, D. Han, M. Xiao, Y. Meng, *Small* **2018**, *14*, 1801420.
[217] J. Rolland, E. Poggi, A. Vlad, J.-F. Gohy, *Polymer* **2015**, *68*, 344.
[218] H. Oh, K. Xu, H. D. Yoo, D. S. Kim, C. Chanthad, G. Yang, J. Jin, I. A. Ayhan, S. M. Oh, Q. Wang, *Chem. Mater.* **2016**, *28*, 188.
[219] C. Z. Zhao, X. Q. Zhang, X. B. Cheng, R. Zhang, R. Xu, P. Y. Chen, H. J. Peng, J. Q. Huang, Q. Zhang, *Proc. Natl. Acad. Sci. USA* **2017**, *114*, 11069.
[220] F. Croce, *Solid State Ionics* **2000**, *135*, 47.
[221] S. Jayanthi, K. Kulasekarapandian, A. Arulsankar, K. Sankaranarayanan, B. Sundaresan, *J. Compos. Mater.* **2015**, *49*, 1035.
[222] O. Sheng, C. Jin, J. Luo, H. Yuan, C. Fang, H. Huang, Y. Gan, J. Zhang, Y. Xia, C. Liang, W. Zhang, X. Tao, *J. Mater. Chem. A* **2017**, *5*, 12934.
[223] K. Liu, F. Ding, J. Liu, Q. Zhang, X. Liu, J. Zhang, Q. Xu, *ACS Appl. Mater. Interfaces* **2016**, *8*, 23668.
[224] A. M. Stephan, T. P. Kumar, M. A. Kulandainathan, N. A. Lakshmi, *J. Phys. Chem. B* **2009**, *113*, 1963.
[225] F. Croce, G. B. Appetecchi, L. Persi, B. Scrosati, *Nature* **1998**, *394*, 456.
[226] F. Croce, S. Sacchetti, B. Scrosati, *J. Power Sources* **2006**, *162*, 685.
[227] S. Tang, W. Guo, Y. Fu, *Adv. Energy Mater.* **2020**, 2000802.
[228] M. A. K. L. Dissanayake, P. A. R. D. Jayathilaka, R. S. P. Bokalawala, I. Albinsson, B. E. Mellander, *J. Power Sources* **2003**, *119-121*, 409.
[229] L. Chen, Y. Li, S.-P. Li, L.-Z. Fan, C.-W. Nan, J. B. Goodenough, *Nano Energy* **2018**, *46*, 176.
[230] K. K. Fu, Y. Gong, J. Dai, A. Gong, X. Han, Y. Yao, C. Wang, Y. Wang, Y. Chen, C. Yan, Y. Li, E. D. Wachsman, L. Hu, *Proc. Natl. Acad. Sci. USA* **2016**, *113*, 7094.
[231] Z. Wan, D. Lei, W. Yang, C. Liu, K. Shi, X. Hao, L. Shen, W. Lv, B. Li, Q.-H. Yang, F. Kang, Y.-B. He, *Adv. Funct. Mater.* **2019**, *29*, 1805301.
[232] J. Zhang, N. Zhao, M. Zhang, Y. Li, P. K. Chu, X. Guo, Z. Di, X. Wang, H. Li, *Nano Energy* **2016**, *28*, 447.
[233] G. Piana, F. Bella, F. Geobaldo, G. Meligrana, C. Gerbaldi, *J. Energy Storage* **2019**, *26*, 100947.
[234] S. Bonizzoni, C. Ferrara, V. Berbenni, U. Anselmi-Tamburini, P. Mustarelli, C. Tealdi, *Phys. Chem. Chem. Phys.* **2019**, *21*, 6142.
[235] J. Zhang, X. Zang, H. Wen, T. Dong, J. Chai, Y. Li, B. Chen, J. Zhao, S. Dong, J. Ma, L. Yue, Z. Liu, X. Guo, G. Cui, L. Chen, *J. Mater. Chem. A* **2017**, *5*, 4940.
[236] W. Liu, S. W. Lee, D. Lin, F. Shi, S. Wang, A. D. Sendek, Y. Cui, *Nat. Energy* **2017**, *2*, 17035.
[237] X. Zhang, T. Liu, S. Zhang, X. Huang, B. Xu, Y. Lin, B. Xu, L. Li, C. W. Nan, Y. Shen, *J. Am. Chem. Soc.* **2017**, *139*, 13779.
[238] J. Yu, Y.-Q. Lyu, J. Liu, M. B. Effat, S. C. T. Kwok, J. Wu, F. Ciucci, *J. Mater. Chem. A* **2019**, *7*, 17995.
[239] J. Yu, S. C. T. Kwok, Z. Lu, M. B. Effat, Y.-Q. Lyu, M. M. F. Yuen, F. Ciucci, *ChemElectroChem* **2018**, *5*, 2873.
[240] W. Zhang, J. Nie, F. Li, Z. L. Wang, C. Sun, *Nano Energy* **2018**, *45*, 413.
[241] X. Tao, Y. Liu, W. Liu, G. Zhou, J. Zhao, D. Lin, C. Zu, O. Sheng, W. Zhang, H. W. Lee, Y. Cui, *Nano Lett.* **2017**, *17*, 2967.
[242] W. Li, C. Sun, J. Jin, Y. Li, C. Chen, Z. Wen, *J. Mater. Chem. A* **2019**, *7*, 27304.
[243] C. Yan, P. Zhu, H. Jia, Z. Du, J. Zhu, R. Orenstein, H. Cheng, N. Wu, M. Dirican, X. Zhang, *Energy Storage Mater.* **2020**, *26*, 448.
[244] K. Pan, L. Zhang, W. Qian, X. Wu, K. Dong, H. Zhang, S. Zhang, *Adv. Mater.* **2020**, *32*, 2000399.
[245] T. H. Wan, Z. Lu, F. Ciucci, in *Encyclopedia of Inorganic and Bioinorganic Chemistry*, John Wiley & Sons, New York **2020**, p. 1.
[246] M. D. Bhatt, C. O'Dwyer, *Phys. Chem. Chem. Phys.* **2015**, *17*, 4799.
[247] M. Park, X. Zhang, M. Chung, G. B. Less, A. M. Sastry, *J. Power Sources* **2010**, *195*, 7904.
[248] J. Liu, Z. Lu, M. B. Effat, F. Ciucci, *J. Power Sources* **2019**, *409*, 94.
[249] K. Xu, *Chem. Rev.* **2014**, *114*, 11503.
[250] O. Borodin, *J. Phys. Chem. B* **2009**, *113*, 11463.
[251] O. Borodin, G. D. Smith, *J. Phys. Chem. B* **2009**, *113*, 1763.
[252] K. Xu, *Chem. Rev.* **2004**, *104*, 4303.
[253] H. Mehrer, *Diffusion in Solids: Fundamentals, Methods, Materials, Diffusion-Controlled Processes*, Springer Science & Business Media, New York **2007**.
[254] T. M. F. Restle, C. Sedlmeier, H. Kirchhain, W. Klein, G. Raudaschl-Sieber, V. L. Deringer, L. van Wullen, H. A. Gasteiger, T. F. Fassler, *Angew. Chem., Int. Ed.* **2019**, *132*, 2.
[255] M. Gauthier, T. J. Carney, A. Grimaud, L. Giordano, N. Pour, H. H. Chang, D. P. Fenning, S. F. Lux, O. Paschos, C. Bauer, F. Maglia, S. Lupart, P. Lamp, Y. Shao-Horn, *J. Phys. Chem. Lett.* **2015**, *6*, 4653.
[256] J. Pan, Y. T. Cheng, Y. Qi, *Phys. Rev. B* **2015**, *91*, 134116.
[257] X. Fan, L. Chen, X. Ji, T. Deng, S. Hou, J. Chen, J. Zheng, F. Wang, J. Jiang, K. Xu, C. Wang, *Chem* **2018**, *4*, 174.
[258] X.-Q. Zhang, X.-B. Cheng, X. Chen, C. Yan, Q. Zhang, *Adv. Funct. Mater.* **2017**, *27*, 1605989.
[259] C. Li, B. Qin, Y. Zhang, A. Varzi, S. Passerini, J. Wang, J. Dong, D. Zeng, Z. Liu, H. Cheng, *Adv. Energy Mater.* **2019**, *9*, 1803422.
[260] X. Fan, X. Ji, F. Han, J. Yue, J. Chen, L. Chen, T. Deng, J. Jiang, C. Wang, *Sci. Adv.* **2018**, *4*, eaau9245.
[261] W. Lai, F. Ciucci, *Electrochim. Acta* **2011**, *56*, 4369.
[262] M. Doyle, J. Newman, *Electrochim. Acta* **1995**, *40*, 2191.
[263] M. Guo, G.-H. Kim, R. E. White, *J. Power Sources* **2013**, *240*, 80.
[264] D. K. Karthikeyan, G. Sikha, R. E. White, *J. Power Sources* **2008**, *185*, 1398.
[265] B. Orvananos, T. R. Ferguson, H. C. Yu, M. Z. Bazant, K. Thornton, *J. Electrochem. Soc.* **2014**, *161*, A535.
[266] T. R. Ferguson, M. Z. Bazant, *J. Electrochem. Soc.* **2012**, *159*, A1967.
[267] T. F. Fuller, M. Doyle, J. Newman, *J. Electrochem. Soc.* **1994**, *141*, 1.
[268] C. Fleischer, W. Waag, H.-M. Heyn, D. U. Sauer, *J. Power Sources* **2014**, *260*, 276.

[269] R. D. Perkins, A. V. Randall, X. Zhang, G. L. Plett, *J. Power Sources* **2012**, *209*, 318.
[270] D. J. Docimo, H. K. Fathy, *J. Electrochem. Soc.* **2017**, *164*, A61.
[271] K. A. Smith, C. D. Rahn, C.-Y. Wang, *Energy Convers. Manage.* **2007**, *48*, 2565.
[272] N. Dawson-Elli, S. B. Lee, M. Pathak, K. Mitra, V. R. Subramanian, *J. Electrochem. Soc.* **2018**, *165*, A1.
[273] P. W. C. Northrop, B. Suthar, V. Ramadesigan, S. Santhanagopalan, R. D. Braatz, V. R. Subramanian, *J. Electrochem. Soc.* **2014**, *161*, E3149.
[274] S. De, P. W. C. Northrop, V. Ramadesigan, V. R. Subramanian, *J. Power Sources* **2013**, *227*, 161.
[275] V. R. Subramanian, V. D. Diwakar, D. Tapriyal, *J. Electrochem. Soc.* **2005**, *152*, A2002.
[276] J. Newman, W. Tiedemann, *AIChE J.* **1975**, *21*, 25.
[277] M. Doyle, T. F. Fuller, J. Newman, *J. Electrochem. Soc.* **1993**, *140*, 1526.
[278] J. S. Newman, C. W. Tobias, *J. Electrochem. Soc.* **1962**, *109*, 1183.
[279] J. Newman, K. E. Thomas, H. Hafezi, D. R. Wheeler, *J. Power Sources* **2003**, *119-121*, 838.
[280] U. S. Kim, C. B. Shin, C.-S. Kim, *J. Power Sources* **2008**, *180*, 909.
[281] Q. Huang, M. Yan, Z. Jiang, *J. Power Sources* **2006**, *156*, 541.
[282] V. Srinivasan, C. Y. Wang, *J. Power Sources* **2002**, *110*.
[283] W. B. Gu, C. Y. Wang, *J. Electrochem. Soc.* **2000**, *147*, 2910.
[284] C. Pals, J. Newman, *J. Electrochem. Soc.* **1995**, *142*, 3282.
[285] C. Pals, J. Newman, *J. Electrochem. Soc.* **1995**, *142*, 3274.
[286] Y. Ji, Y. Zhang, C. Y. Wang, *J. Electrochem. Soc.* **2013**, *160*, A636.
[287] G.-H. Kim, A. Pesaran, R. Spotnitz, *J. Power Sources* **2007**, *170*, 476.
[288] R. Spotnitz, J. Franklin, *J. Power Sources* **2003**, *113*, 81.
[289] C. Zhang, S. Santhanagopalan, M. A. Sprague, A. A. Pesaran, *J. Power Sources* **2015**, *290*, 102.
[290] X. Feng, M. Ouyang, X. Liu, L. Lu, Y. Xia, X. He, *Energy Storage Mater.* **2018**, *10*, 246.
[291] R. M. Spotnitz, J. Weaver, G. Yeduvaka, D. H. Doughty, E. P. Roth, *J. Power Sources* **2007**, *163*, 1080.
[292] J. Kim, J. Oh, H. Lee, *Appl. Therm. Eng.* **2019**, *149*, 192.
[293] M. B. Effat, C. Wu, F. Ciucci, *Asia-Pac. J. Chem. Eng.* **2016**, *11*, 399.
[294] G. Bucci, B. Talamini, A. Renuka Balakrishna, Y.-M. Chiang, W. C. Carter, *Phys. Rev. Mater.* **2018**, *2*, 105407.
[295] C. Monroe, J. Newman, *J. Electrochem. Soc.* **2004**, *151*, A880.
[296] C. Monroe, J. Newman, *J. Electrochem. Soc.* **2005**, *152*, A396.
[297] G. Stone, S. Mullin, A. Teran, D. Hallinan, A. Minor, A. Hexemer, N. Balsara, *J. Electrochem. Soc.* **2012**, *159*, A222.
[298] K. J. Harry, K. Higa, V. Srinivasan, N. P. Balsara, *J. Electrochem. Soc.* **2016**, *163*, A2216.
[299] R. Khurana, J. L. Schaefer, L. A. Archer, G. W. Coates, *J. Am. Chem. Soc.* **2014**, *136*, 7395.
[300] Z. Hong, V. Viswanathan, *ACS Energy Lett.* **2018**, *3*, 1737.
[301] Y. Gao, H. Zhao, D. Chen, C. Chen, F. Ciucci, *Carbon* **2015**, *94*, 1028.
[302] P. Barai, K. Higa, V. Srinivasan, *Phys. Chem. Chem. Phys.* **2017**, *19*, 20493.
[303] D. A. Cogswell, *Phys. Rev. E: Stat., Nonlinear, Soft Matter Phys.* **2015**, *92*, 011301.
[304] A. D. Sendek, Q. Yang, E. D. Cubuk, K.-A. N. Duerloo, Y. Cui, E. J. Reed, *Energy Environ. Sci.* **2017**, *10*, 306.
[305] A. D. Sendek, E. D. Cubuk, E. R. Antoniuk, G. Cheon, Y. Cui, E. J. Reed, *Chem. Mater.* **2019**, *31*, 342.
[306] Y. Zhang, X. He, Z. Chen, Q. Bai, A. M. Nolan, C. A. Roberts, D. Banerjee, T. Matsunaga, Y. Mo, C. Ling, *Nat. Commun.* **2019**, *10*, 5260.
[307] A. Ishikawa, K. Sodeyama, Y. Igarashi, T. Nakayama, Y. Tateyama, M. Okada, *Phys. Chem. Chem. Phys.* **2019**, *21*, 26399.
[308] Y. Okamoto, Y. Kubo, *ACS Omega* **2018**, *3*, 7868.
[309] M. Shelton, S. Venkatram, R. Ramprasad, presented at 236th ECS Meeting. The Electrochemical Society **2019**.
[310] Z. Ahmad, T. Xie, C. Maheshwari, J. C. Grossman, V. Viswanathan, *ACS Cent. Sci.* **2018**, *4*, 996.
[311] C. Chen, W. Ye, Y. Zuo, C. Zheng, S. P. Ong, *Chem. Mater.* **2019**, *31*, 3564.
[312] A. Jain, S. P. Ong, G. Hautier, W. Chen, W. D. Richards, S. Dacek, S. Cholia, D. Gunter, D. Skinner, G. Ceder, K. A. Persson, *APL Mater.* **2013**, *1*, 011002.
[313] K. Hatakeyama-Sato, T. Tezuka, M. Umeki, K. Oyaizu, *J. Am. Chem. Soc.* **2020**, *142*, 3301.
[314] Z. Dai, J. Yu, J. Liu, R. Liu, Q. Sun, D. Chen, F. Ciucci, *J. Power Sources* **2020**, *464*, 228182.
[315] Y. Cui, J. Wan, Y. Ye, K. Liu, L. Y. Chou, Y. Cui, *Nano Lett.* **2020**, *20*, 1686.
[316] Y. Li, Y. Li, A. Pei, K. Yan, Y. Sun, C.-L. Wu, L.-M. Joubert, R. Chin, A. L. Koh, Y. Yu, J. Perrino, B. Butz, S. Chu, Y. Cui, *Science* **2017**, *358*, 506.
[317] A. V. Chadwick, S. L. Savin, R. Alcantara, D. Fernandez Lisbona, P. Lavela, G. F. Ortiz, J. L. Tirado, *ChemPhysChem* **2006**, *7*, 1086.
[318] W. C. Chueh, F. El Gabaly, J. D. Sugar, N. C. Bartelt, A. H. McDaniel, K. R. Fenton, K. R. Zavadil, T. Tyliszczak, W. Lai, K. F. McCarty, *Nano Lett.* **2013**, *13*, 866.
[319] S. Nishimura, G. Kobayashi, K. Ohoyama, R. Kanno, M. Yashima, A. Yamada, *Nat. Mater.* **2008**, *7*, 707.
[320] S. Kaboli, H. Demers, A. Paolella, A. Darwiche, M. Dontigny, D. Clement, A. Guerfi, M. L. Trudeau, J. B. Goodenough, K. Zaghib, *Nano Lett.* **2020**, *20*, 1607.

Xidong Lin obtained his Ph.D. degree in polymer chemistry and physics with Prof. Dingcai Wu at Sun Yat-sen University in 2018. He joined Prof. Francesco Ciucci's group in The Hong Kong University of Science and Technology as a post-doctoral fellow in 2019. His research interest focuses on the development of novel electrolyte materials for rechargeable batteries.

Guodong Zhou received his B.Eng. and M.Eng. from Zhejiang University. Currently, he is a Ph.D. student in the Department of Mechanical and Aerospace Engineering at The Hong Kong University of Science and Technology under the supervision of Prof. Francesco Ciucci. His research focuses on new electrolytes for Li-ion batteries and lithium metal batteries.

Francesco Ciucci is an associate professor at The Hong Kong University of Science and Technology. He obtained his Ph.D. from the California Institute of Technology, USA, and did his postdoctoral work at the University of Heidelberg, Germany. Francesco's current research centers on solid-state energy technologies, including solid-oxide fuel cells, electrolyzers, and solid-state batteries, with particular emphasis on the modeling of these systems and the development of new functional materials.